A review of experimental methods for nucleation rate determination in large volume batch and microfluidic crystallization

Cedric Devos, Tom Van Gerven, Simon Kuhn*

KU Leuven, Department of Chemical Engineering, Celestijnenlaan 200F, 3001 Leuven, Belgium

ABSTRACT: Experimental nucleation rate determination for crystallization in solution has been acknowledged as an important topic for a long time, as it improves the design and control of industrial crystallization processes, and offers insights into the mechanisms of nucleation. Characterization of nucleation rates in large volume batch crystallizers has been widely studied in the past, which has led to the development of a variety of models linking the nucleation rate to the metastable zone width and induction time. These methods remain important due to their role in industrial crystallization. More recently, the use of microfluidic platforms has resulted in the development of methods to obtain nucleation rates based on the stochastic nature of nucleation. This has opened new pathways for understanding nucleation on a molecular level. This review presents a critical overview of nucleation rate determination methods: large volume batch crystallizer models (Part I), and microfluidic and microvial models (Part II) are presented in terms of equations, advantages and limitations. Published experimental nucleation rate values are summarized (SI). A critical discussion of experimental nucleation rate determination is given (Part III). The objective of the review is to be a starting point for researchers attempting to experimentally characterize nucleation behavior.

INTRODUCTION

Crystallization is one of the most important separation and purification techniques in the pharmaceutical industry. More than 90% of all pharmaceutical products contain crystallized solids[1]. Traditionally, crystallization is divided in two steps: nucleation and growth. Nucleation is the first step, during which a small crystal nucleus is formed, and therefore has an important influence on the subsequent steps and the final crystal product properties[2,3]. To date, the formation of a nanoscopically small crystal nucleus[2] remains a mystery, but indirect methods to measure nucleation kinetics have been developed. In the past, nucleation kinetics were measured primarily with the objective of improving the design and control of industrial large volume batch crystallization processes. The development of microfluidic technology has resulted in new methods to characterize the first stages of crystallization. The attention of nucleation kinetics determination has shifted towards unravelling the mechanistic steps of nucleation on a molecular level. This shift is reflected in the books and reviews about crystal nucleation experiments. For example Nývlt *et al.* gave an overview of the field in 1985 in their book "The Kinetics of Industrial Crystallization"[4]. In 1987, Tavare wrote a general review about batch crystallization with a focus on extracting nucleation and growth kinetics[5]. Eight years later, Tavare presented nucleation and growth kinetics as an important "concept" to analyze industrial crystallizers[6]. In 2002, Garside, Mersmann and Nývlt published "Measurement of Crystal Growth and Nucleation Rates (2nd Edition)" "stimulated by the […] need in a wide range of industries"[7]. The main advantage of this book, according to Mullin, is that it provides an advantage in the design and control of crystallizers[7]. The molecular understanding of nucleation, on the other hand, was studied experimentally mainly via vapor to liquid nucleation experiments, with diffusion cloud chambers, expansion chambers, shock tubes, supersonic nozzles, etc.[8–10]. Since the beginning of this century, the use of microfluidic technology has led to the development of methods to determine the nucleation kinetics in solution in very small volumes. These results give more information about primary nucleation and have since been used to improve the understanding of nucleation in solution. In 2013, Davey *et al.* gave an overview of recent reviews with a focus on the molecular mechanism of nucleation[11].

With 'nucleation rates' becoming a hot topic again, we present a critical review about experimental methods for the determination of nucleation rate parameters for solution crystallization of organic molecules and proteins. The need for a review about nucleation rate kinetics in solution was recognized by Xiao *et al.,* in 2018. They published a review about nucleation rate determination methods in solutions for investigating the nucleation process[12]. They present five methods: the deterministic method, the droplet-based method, the double-pulse method, the microfluidic method and the stirred small volume solution method[12]. We abandon the five methods framework suggested by Xiao *et al.*[12] and make a distinction between (i) large volume batch crystallizers (in **Part I**) and (ii) small volume microfluidic and microvial models (in **Part II**). Methods that try to determine the nucleation rate theoretically or by simulations are out-of-scope (*e.g.* population balance equation (PBE) models[13], Monte Carlo[14] or molecular dynamic simulations[15]). The models for each group are discussed in detail and reviewed critically in terms of advantages and limitations.

Part I of this review focusses on isothermal and polythermal batch crystallizer models. These models link the metastable zone width and cooling rate or induction time to the nucleation kinetics via (generally empirical) equations. To our knowledge no review has been published that summarizes these methods completely. Special attention goes to the polythermal model published by Nývlt (known as the Nývlt equation)[16] and the models that adapt and improve upon this model (e.g. Kubota[17,18], Sangwal[19,20]). These methods are becoming more outdated, but understanding the models and their limitations remains crucial in order to interpret the older papers. In addition, they remain a fast and usually relatively simple way to quickly characterize the nucleation (or crystallization) process. Also, for these models the shift towards an improved understanding can be noticed, for example with the development of the KBHR model in 2010[21,22]. In **Part II,** the microfluidic and microvial models are described in detail and critically examined. These models rely on the stochastic nature of nucleation that is observed in polythermal and isothermal experiments in small volumes. The experimental data is linked to theoretical probability equations and the nucleation kinetics. As the field of uncovering the molecular mechanisms of nucleation is evolving further, it is also important to critically look at the current published literature. As more and more experimental nucleation data is generated, quantitative comparisons between process conditions can accelerate discoveries. Therefore, tables of published data are presented in this review for different microfluidic methods in the **SI**. Finally, in **Part III** a critical discussion of nucleation rate experiments is given.

NUCLEATION

There are different types of nucleation. Apart from primary homogeneous or spontaneous nucleation, nucleation can also occur due to impurities or dust present in the solution or on the walls of the crystallizer. This is called primary heterogeneous nucleation. If nucleation is induced by the presence of solute crystals it is called secondary nucleation.

Homogeneous nucleation

How nucleation, the birth of a new crystal nucleus, exactly happens remains unknown[23]. The Classical Nucleation Theory (CNT) is the most popular framework to explain nucleation[24]. Small concentration fluctuations in a supersatured liquid cause the formation of small and extremely unstable embryos by molecular addition. Most of these embryos dissolve again, but those in regions of local high supersaturations can continue to grow and reach the critical size. The embryos that reach the critical size have a chance to overcome the free energy barrier and become a crystal via a chain reaction[23], as shown in Figure 1. The thermodynamic basis of the CNT is developed by Gibbs[23], the kinetic part of the theory was proposed in the first half of the 19th century by Volmer and Weber (1926) and later extended by Becker, Döring and many others[25]. For a complete description of the CNT we refer to Kashchiev's book[26].

The core assumption of the CNT is the classical capillarity approximation, which says that small clusters, nuclei and droplets can be treated as macroscopic objects and can be described using bulk properties[27,28]. Clusters are assumed to have a well-defined radius and interfacial energy. In the CNT, the nucleation process is viewed as a series of single molecule additions to the nucleus. It is assumed that the attachment of a molecule does not influence any successive attachments[27]. The chemical potential change of the solute ($\Delta\mu$) is the thermodynamic driving force of nucleation, which is expressed through the supersaturation, S ($\frac{\Delta\mu}{R_G T} = \ln\left(\frac{a_i}{a_{i,sat}}\right) = \ln(S)$) [23,29]. The nucleation rate (J) (number of nuclei per volume per time) is defined as an Arrhenius equation, as is shown in eq. 1, with A the kinetic nucleation parameter, k_b the Boltzmann constant, γ the crystal-solution interfacial tension and ν the molecular volume (approximated by $M_W/\rho N_A$). Eq. 1 can be simplified into eq. 2, with B the thermodynamic nucleation parameter. The nucleation rate as discussed here is for interface-transfer limited nucleation, other common nucleation rate expressions are summarized in the SI.

$$J = A\exp\left(-\frac{16\pi\gamma^3 v^2}{3k_b^3 T^3 \ln^2(S)}\right) = \mathrm{A}\exp\left(-\frac{4\pi r_{crit}^2\cdot\gamma}{3k_b T}\right) \quad (1)$$

$$J(S) = AS\cdot\exp\left(-\frac{B}{\ln^2(S)}\right) \quad (2)$$

If the nuclei are assumed to be spherical, eq. 3 is obtained. The kinetic nucleation parameter can then be written as is shown in eq. 4.

$$B = \frac{16\pi\cdot\gamma^3\cdot v^2}{3k_b^3 T^3} \quad (3)$$

$$A = \frac{f^* c_0 z}{S} \quad (4)$$

With f^* the attachment frequency, c_0 the concentration of active nucleation sites, and z the Zeldovich factor, which accounts for the fact that not all critical clusters continue to grow into large crystals. It is usually assumed that f^* is the rate-limiting step for nucleation in solution[11]. The simplicity of the CNT is attractive, but it lacks a desired predictive nature. A values estimated with the CNT are between 10^{25}m^{-3}s^{-1} and 10^{30}m^{-3}s^{-1} [11,24,30], whereas A values estimated from experimental data are significantly lower, usually between 10 and 10^7m^{-3}s^{-1}. This difference may arise because of the invalidity of the capillary approximation[31]. For a more in-depth explanation of the thermodynamic and pre-exponential kinetic factor we refer to ref. [32].

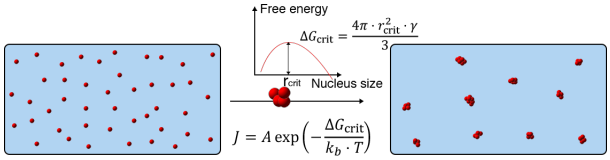

Figure 1 Graphical representation of the CNT in solution

Two-step nucleation

In the CNT, density and structure fluctuations are implicitly assumed to occur simultaneously[33], but this does not always seem to be the case in reality[1,33]. Based on simulations, but later verified using nucleation data of the model protein lysozyme[33,34], a nonclassical phenomenological model for nucleation has been proposed: the two-step nucleation model. According to this model nucleation takes place in two steps: (i) the formation of a dense droplet; and (ii) nucleation inside this dense droplet. The density fluctuations occur before the structural fluctuations. The two-step nucleation model predicts an exponential dependency of the nucleation rate on the supersaturation, but once a critical

supersaturation is reached the nucleation rate decreases or levels-off[33,35]. This "breaking nucleation rate J(c)" has been experimentally observed[24]. The two-step model enables the explanation of experimental observations, for which the CNT fails. For protein crystallization the second step is the rate-limiting step[36]. Nevertheless, true insight in the molecular phenomena remains difficult even with nonclassical models[11].

Heterogeneous nucleation

Impurities can act as heterogeneous nucleation sites. The energy barrier for nucleation is lowered and nucleation can occur at lower supersaturations. The kinetic nucleation factor is related to the concentration of active nucleation sites c_0, as shown in eq. 4. The ratio of the pre-exponential nucleation factor for homogeneous nucleation and heterogeneous nucleation is proportional to the concentration of active "homogeneous nucleation sites" (assumed to be the concentration of molecules) and active heterogeneous nucleation sites (impurities present in the solution), as is shown in eq. 5.

$$\frac{A_{\mathrm{HO}}}{A_{\mathrm{HE}}} \approx \frac{c_{0,\mathrm{ho}}}{c_{0,\mathrm{he}}} \tag{5}$$

Isothermal and polythermal experiments

According to the CNT, nucleation commences from the moment supersaturation is generated. Generally however, a certain time elapses between the generation of supersaturation and detection of the first crystals in the solution. The system is in a metastable state. Two kinetic properties are introduced to quantify the ability of the system to remain in this metastable state[37] : the metastable zone width (MZW) and the induction time.

The MZW, first introduced by Ostwald in 1897[38], is the temperature difference between the saturation temperature and the temperature at which nucleation occurs for a constant cooling rate. The mathematical and graphical description of the MZW is respectively given in eq. 6, and Figure 2[39]. The induction time (t_{ind}) is the time difference between the moment of supersaturation generation and the detection of crystals for a constant supersaturation. According to Mullin, the induction time is considered to consist of different contributions[23]: t_r the relaxation time required for the system to achieve a quasi-steady-state distribution of clusters; t_n, the nucleation time required for the formation of the critical nuclei; and t_g the growth time required for crystals to grow from the critical size to a detectable crystal[23]. This definition of the induction time is shown in eq. 7, but also other definitions are used in literature.

$$\Delta T_{\mathrm{max}} = T_{\mathrm{det}} - T_{\mathrm{eq}} \tag{6}$$

$$t_{\mathrm{ind}} = t_r + t_n + t_g \tag{7}$$

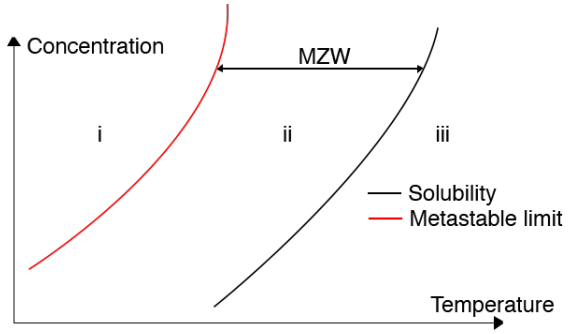

Figure 2 Miers phase diagram with three different zones, after Myerson *et al.*[39]: (i) labile zone: supersaturated region with spontaneous homogeneous nucleation and growth, (ii) metastable zone: supersaturated region with growth and no homogeneous spontaneous nucleation, (iii) stable zone: undersaturated region with no crystallization.

A distinction is made between polythermal and isothermal experiments, which is graphically illustrated in Figure 3. For polythermal (or MZW) experiments, a solution is cooled at a constant cooling rate, until crystals are detected. For isothermal (or induction time) experiments, the temperature is kept constant throughout the experiment from the moment the supersaturation is generated. The time from the start of the experiment until the appearance of crystals is recorded. Isothermal and polythermal experiments generally require similar setups, time and effort[40]. It is therefore recommended to choose the method with the largest experimental range as the main method, with the other optionally used as a check[40].

It is well known that the accuracy of these experiments depends strongly on the crystal detection technique[18]. The formation of a critical cluster can involve as little as a few tens of molecules[41]. To observe this, detection methods with extreme resolution are required which currently do not exist. Hence, there is always a time lag between the moment of nucleation and the moment of detection, during which crystals grow to a detectable size[5,17,42,43]. The analytical detection methods are divided into three categories: methods relying on image analysis, detection of the first crystal, methods detecting a change in solution concentration. An overview is shown in Table 1.

Table 1 Analytical techniques for crystal detection, followed by references in which the technique is used.

Image analysis
Particle vision measurements (PVM) (e.g. Lasentec PVM)[43]
Blaze probe
EasyViewer Probe
External bulk video imaging (eBVI)[44]
Optical microscopy[45,46] – inline video microscopy (IVM)
Detection of the first crystal
Light transmission (e.g. Crystal16[2]/Crystalline, colorimeter)[47,48]
FBRM[49] (e.g. Lasentec "ParticleTrack" probe)[42,43,48,50]
Naked eye[49]
Turbidity via in-situ camera[51,52]
3D Optical reflectance measurement (ORM)[53]
Turbidity probe[54]
Detection of changes in the solution concentration
FTIR spectrometer[49]
Ultrasound (US) sensor[55–57]
Electrical conductivity[58] (oscilloscope)[23]
Raman spectrometer[53]
Electrozone sensing (Coulter counter)[59]
Density measurements (densitometer)[60]
Refractive index[58]
Dielectric constant[48]
Other
Heat of crystallization[61]

The accuracy of each method is dependent on the minimum size of crystals that can be detected, and the number of crystals required for detection. Methods relying on changes in the solution concentration are most prone to large experimental errors, as many crystals must be present. Methods making use of image analysis can detect as little as a single crystal and are generally considered accurate. Methods relying on the detection of the first crystal can also detect a single crystal if it is in the detectable size range (*e.g.* FBRM: 0-20μm [43]), but may also require a threshold crystal concentration (*e.g.* light transmission may require a specific volumetric holdup of crystals). FBRM (stationary focal point) and 3D ORM (dynamic focal point) measure the chord length distribution, which can be related to the particle size distribution. Turbidity measurements generally refer to detection of the point at which the solution turns turbid (cloudy).

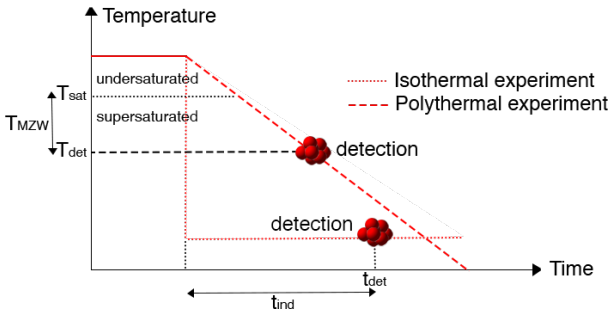

Figure 3 Graphical representation of isothermal and polythermal experiments for cooling crystallization.

Stochastic nature of nucleation

The formation of the critical nucleus is an intrinsic stochastic process[62,63], caused by random spontaneous density and structural fluctuations in the solution[29,64]. There is abundant experimental evidence for this stochasticity in small volumes[2,62,65,66]. The probability of nucleation in an infinitesimal time step is defined as $\kappa(t)dt$, with $\kappa(t)$ the time-dependent rate of nucleation[64]. The equation $\kappa = JV$ links the probability of nucleation to the macroscopic nucleation rate from the CNT[64]. The number of nuclei formed is dependent on the nucleation rate (J), the solution volume, and the time; as shown in eq. 8.

$$N = JV \cdot t \tag{8}$$

The stochastic nature of nucleation becomes apparent experimentally for small JV-values (*e.g.* below 100-1000mL)[67], as is graphically represented in Figure 4. This is reflected by a variation in induction times or MZWs. Models have been developed to extract the nucleation rate J from this variation, with the Markovian Poisson description being the most popular. In larger volume crystallizers the probability of nucleation (JV) is high. Hence, the variance in recorded induction times or MZWs is not observed in large batch crystallizers.

The Markovian approximation assumes that the system goes from m nuclei to $m+1$ nuclei (single step transitions) and that the rate of formation is independent of the amount of already existing nuclei[64]. Further, it is assumed that nucleation of a nucleus does not deplete the supersaturation. The probability of forming m nuclei (N) independently from each other in a time interval (at constant supersaturation) is described in eq. 9[2,68].

$$P_m = \frac{N^m}{m!} \cdot \exp(-N) \tag{9}$$

The probability of zero nuclei being formed in a time interval ($m=0$) is shown in eq. 10[2]. The

probability of at least 1 nucleus being formed is shown in eq. 11. Substitution of eq. 8 in eq. 11 gives the probability of at least 1 nucleus being formed (corrected for a crystal growth time (t_g)), as shown in eq. 12.

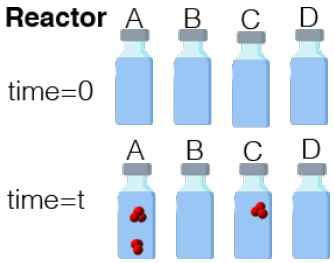

Figure 4 Graphical representation of the stochastic nature of nucleation in microvial crystallizers.

$$P_0 = \exp(-N) \quad (10)$$

$$P_{\geq 1} = 1 - \exp(-N) \quad (11)$$

$$P(t) = 1 - \exp\left[-JV \cdot \left(t - t_g\right)\right] \quad (12)$$

The growth time is usually considered to be a deterministic property (which is incorrect for growth rate dispersion[69]), that is dependent on the supersaturation and independent of the volume. Eq. 12 can be extended with the relaxation time t_r. These theoretical equations are (usually least-squares) fitted to experimental cumulative probabilities to obtain the nucleation rate and the growth time. If the nucleation rate for different supersaturation ratios is determined, the logarithm of the CNT nucleation rate equation can be taken to obtain eq. 13. This equation is dependent on the CNT nucleation rate expression. A plot of $\ln(J/S)$ against $\ln^{-2}(S)$ results in a slope of $-B$ and an intersection with the y-axis at $\ln(A)$ [69].

$$\ln\left(\frac{J}{S}\right) = \ln(A) - B \cdot \ln^{-2}(S) \quad (13)$$

Isothermal experiments are described by a homogeneous Poisson process, whereas polythermal experiments (*e.g.* cooling crystalliztion) are described by an inhomogeneous Poisson process. The cumulative probability *P(t)* that nucleation has occurred before time t for changing supersaturations is shown in eq. 14. For polythermal experiments, the nucleation rate is assumed to be constant during one time step, but is changing during successive time steps (because the supersaturation changes)[64]. These time steps are assumed to be short, but just long enough for the system to reach equilibrium[64]. Other more advanced models can be found in literature (*e.g.* two models for batch cooling crystallization proposed by Maggioni and Mazzotti)[62].

$$P(t) = 1 - \exp\left(-V \cdot \int_0^{t-t_g} J\left(t - t_g\right) d\left(t - t_g\right)\right) \quad (14)$$

Mono- and polynuclear nucleation mechanisms

There are two theories to explain how a supersaturated system loses its metastability: the polynuclear nucleation mechanism (PNM); and the mononuclear nucleation mechanism (MNM)[37]. The PNM assumes simultaneous appearance of several nuclei, which then grow to a detectable size. The MNM assumes that only a single nucleus appears in the solution. Both mechanisms are boundary cases: the MNM accurately describes small (microfluidic) volumes and the PNM describes large volume crystallization processes.

The MNM is closely related to the single nucleation mechanism (SNM), which assumes that a single primary nucleus is formed which grows to a fixed size[70]. Once this nuclei has reached the minimum size other nuclei are formed via secondary nucleation (which is assumed to happen due to abrasion or attrition by crystal-impeller collisions[70,71]). The SNM has been observed experimentally, *e.g.* in a droplet-based microfluidic platform[72] and in a microvial[71].

PART I: LARGE VOLUME BATCH CRYSTALLIZERS

Most industrial crystallization processes use stirred batch crystallizers[73]. Nucleation rate determination in these crystallizers is difficult, due to the interplay between different control parameters and nucleation mechanisms. The mathematical data analysis methods usually rely on questionable assumptions, failing to take into account the complexity of the problem[74]. This Section examines different data analysis methods for polythermal and isothermal experiments performed in large volume batch crystallizers. These methods can capture the experimental data well, but generally do not provide physical insight into the mechanisms of nucleation. Table 2 gives an overview of the different methods. The Nývlt equation links the cooling rate to the MZW via a power law for the nucleation rate (eq. 15), and is used to analyze polythermal experiments[16]. Since then, attempts have been made to improve the Nývlt-equation: make it more physically rigorous (*e.g.* the methods developed by Kubota and Sangwal[17,19]), or propose completely different equations (*e.g.* the KBHR method, and the second method by Sangwal[20,21]). As crystallizers are usually large, nucleation is considered as a deterministic event (a notable exception is the stochastic model proposed by Kubota[17]). We attempt to give an overview of newer and older

methods, but not all approaches are discussed in detail: *e.g.* in-depth discussion of the relationships between MZW and nucleation kinetics developed by Mullin and Jančić (1979) and Söhnel and Mullin (1988) are omitted[23]. For each polythermal and isothermal method a short list of advantages and disadvantages is given. It is usually assumed that nucleation does not deplete supersaturation (because nuclei are extremely small), that solutions are uniformly mixed (not too viscous solutions) and that the latent heat of crystallization can be removed sufficiently. In all methods spherical nuclei are generally assumed, but expressions for different shapes can be found easily. Furthermore, it is generally assumed that *A, B* are independent of the temperature. The supersaturation (S) is usually assumed to be the ratio of the concentrations (in mole fractions or concentration fractions), which may affect the accuracy. All polythermal methods assume the cooling rate is not extremely large.

$$J = k\,\Delta c_{\max}^{n} = k'\Delta T_{\max}^{n} \tag{15}$$

Table 2 Overview of data analysis methods for the determination of the nucleation kinetics in large volume batch crystallizers for isothermal and polythermal experiments, and the page number where these methods are discussed in this review.

Large volume batch crystallizer isothermal and polythermal data analysis methods	**Pg.**
Preckshot *et al.* i**sothermal** method (1952)[75]	14
Nývlt **polythermal** model (1969)[16]	7
Söhnel and Nývlt: first crystal **polythermal** model (1976)[76]	7
Söhnel and Nývlt: cloud of crystals **polythermal** model (1976)[76]	7
Harano *et al.* **isothermal** method (1976)[77,78]	14
Mullin and Jančić **polythermal** method (1979)[23]	-
Harano *et al.* **polythermal** method (1981)[79]	14
Mullin and Söhnel **polythermal** method (1988)[23]	-
Mersmann and Bartosch **polythermal** model (seeded nucleation) (1998)[80]	10
Kashchiev *et al.* **isothermal** method (1991)[37]	12
Kim and Mersmann **polythermal** model (2001)[81]	10
Kubota stochastic **polythermal** model (2004)[17]	8
Kubota deterministic **polythermal** model (2004)[17,18]	7
Kubota **isothermal** deterministic model (2008)[18]	8
Nývlt-like equation by Nagy *et al.* method (2008)[82]	13
Sangwal's **polythermal** self-consistent Nývlt-like equation (2009)[19]	8
Sangwal's second **polythermal** model (2009)[20]	9
KBHR **polythermal** and **isothermal** model (2010)[21,22]	11
Shiau **polythermal** and **isothermal** methods (2014, 2018)[83,84]	14

The Nývlt equation

Based on the CNT, Nývlt derived the nucleation rate as a power law in mass basis[16] (J_m [g/h]), with k the nucleation rate and n the nucleation order, as is shown in eq. 16. The relationship between the MZW and the maximum concentration difference is assumed to be as is shown in eq. 17.

$$J_m = k_m \Delta c_{\max}^{n} \tag{16}$$

$$\Delta c_{\max} = \frac{dc_{\mathrm{eq}}}{dT} \cdot \Delta T_{\max} \tag{17}$$

Nývlt then assumed the nucleation rate to be proportional to the "supersaturation rate" (at least for the short period of time in which nucleation takes place)[16]. This newly defined supersaturation rate is related to the cooling rate (q) and a parameter M, defined as the "crystal mass deposited per unit mass of 'free' solvent when the solution is cooled by 1°C", as is shown in eq. 18[23].

$$J_m = M \cdot q \tag{18}$$

M can be rewritten in terms of a parameter ε, which is a function of R_N ("the ratio of molecular weights of the hydrate and anhydrous salt"[23]) and c_N ("the solution concentration expressed as mass of anhydrous per unit mass of solvent at a certain temperature"[23]), as is shown in eq. 19.

$$M = \frac{\varepsilon dc_{\mathrm{eq}}}{dT}, \varepsilon = \frac{R_N}{\left(1 - c_N \cdot (R_N - 1)\right)^2} \tag{19}$$

The well-known Nývlt equation is obtained by substituting eqs. 18 and 19 in eq. 17 and taking the logarithm. Nucleation order and nucleation rate can then be found by plotting $\log(q)$ against $\log(\Delta T_{\max})$. The Nývlt equation, shown in eq. 20, is the first equation to link the MZW and the cooling rate and is still used to this day, but the equation is also heavily criticized (see disadvantages).

$$\log(q) = (n-1) \cdot \log\left(\frac{dc_{\mathrm{eq}}}{dT}\right) - \log(\varepsilon) + \log(k_m) + n \cdot \log(\Delta T_{\max}) \tag{20}$$

Advantages: (i) The method is simple to use, even more so if ε is assumed to be 1. **(ii)** The method has been applied frequently. **Disadvantages: (i)** Neither nucleation order, nor rate have any physical meaning. According to Nývlt *et al.* the nucleation parameters are dependent on physiochemical properties of the solutes, for a more in depth analysis we refer to their paper[85]. **(ii)** Nývlt assumes that the nucleation rate is proportional to the 'supersaturation rate', but this neglects the depletion of supersaturation due to growth of crystal nuclei[86]. Söhnel and Nývlt tried to solve this problem by assuming a certain period of time is required for the growth of a nuclei to a detectable size (the first crystal model)[76]. The growth rate is then assumed to be a power law with exponent g and growth rate constant k_g. Söhnel and Nývlt found that plotting $\log(q)$ versus $\log(\Delta T_{\max})$ results in a slope of $(3g + 3+n)/3$ rather than n (like in the classical Nývlt equation)[76]. If the MZW is detected by the appearance of a "cloud of crystals" rather than the appearance of a first crystal (cloud of crystals model) a slope $(3g+4+n)/4$ is obtained by plotting $\log(q)$ against $\log(\Delta T_{\max})$[23,76]. This result is identical to the one found by Hulburt (using a PBE)[87]. A complete derivation of both the first crystal model and the cloud of crystals model can be found in the paper by Söhnel and Nývlt[76]. The nucleation rate order from the classical Nývlt equation can be considered as an "apparent nucleation rate order". **(iii)** Nývlt assumes that dc_{eq}/dT is independent of the temperature (linear solubility-temperature relationship). **(iv)** It is assumed that the (spherical) nuclei are isolated[88]. **(v)** A final problem is the definition of the nucleation rate in mass basis, which leads to unusual units for k and is inconsistent with other literature where the nucleation rate is defined as the number of nuclei per volume per time. There are formulas to transform the mass based nucleation rate constant to a numbers based constant (with the nucleation order unchanged), if the volume shape factor and crystal density are known and a reasonable assumption of the critical radius can be made[18,89]. Nývlt does not use the nucleation rate as defined by the CNT but proposes a (semi-)empirical power law.

Deterministic approach by Kubota

Kubota proposed two non-conflicting models to correlate the MZW and the cooling rate[17]: one deterministic model and one stochastic model. The advantage of Kubota's approaches is that it accounts for the detection method. Kubota defined the nucleation rate J using a power law, with k the nucleation rate and n the nucleation order, as is shown in eq. 15.

The total number of crystals (N_m) nucleated in a time (t_{end}) can be calculated, as shown in eq. 21.

$$N_m = \int_0^{t_{\mathrm{end}}} JV\, dt \tag{21}$$

For a constant cooling rate ($q = d\Delta T/dt$) the total number of crystals nucleated at the point of the MZW is shown in eq. 22. Taking the logarithm of both sides results in eq. 23.

$$N_m = \int_0^{\Delta T_{\max}} \frac{JV}{q}\, d\Delta T = \frac{k'V}{q(n+1)} \Delta T_{\max}^{n+1} \tag{22}$$

$$\log(\Delta T_{\max}) = \frac{1}{n+1}\log\left(\frac{N_m}{V}\right) + \frac{1}{n+1}\log\left(\frac{n+1}{k'}\right) + \frac{1}{n+1}\log(q) \tag{23}$$

For Kubota's approach the formulas are given in terms of $\log(\Delta T_{\max})$ vs $\log(q)$ rather than the other way around, but the formulas can be easily transformed. The nucleation rate k and order n can be found by plotting $\log(\Delta T_{\max})$ against $\log(q)$.

Advantages: (i) Kubota takes into account the detection method by using the turbidity (N_m/V). The slope and intercept of Kubota's deterministic equation can be considered to be independent of the detection method. **(ii)** The simplicity of the approach makes it an attractive alternative to the Nývlt-equation. **(iv)** Kubota argues, that because of the lower supercooling only primary nucleation will occur[17], but the power law equation can also be used to describe other nucleation mechanisms. **(v)** Kubota also proposed an isothermal analysis method (eq. 25) which can be used to double-check results[18]. **Disadvantages: (i)** Assumptions must be made on the correct value of (N_m/V). The method assumes that the detection method is only dependent on N_m/V. **(ii)** Kubota uses an empirical power law, which does not rely on the CNT: neither nucleation order, nor nucleation rate are physically sensible. They are the same parameters as in Kubota's stochastic model. **(iii)** The model does not take into account the depletion of the supersaturation due to growth. **(iv)** In eq. 15 a linear solubility-temperature relationship is assumed.

Kubota also proposed an isothermal data analysis method, based on the number density (N_m/V) [18]. The nucleation rate is assumed to follow the power law from eq. 15. This results in eq. 26. Eq. 24 can then be integrated and rearranged, which results in eq. 25[18].

$$\frac{N_m}{V} = \int_0^{t_{\text{ind}}} J\, dt = \int_0^{t_{\text{ind}}} k'^{(\Delta T)^n} dt \qquad (24)$$

$$t_{\text{ind}} = \left(\frac{N_m}{k'V}\right) \cdot (\Delta T)^{-n} \qquad (25)$$

Stochastic approach by Kubota

Kubota's stochastic polythermal model also defines the nucleation rate as a power law (eq. 15). As the cooling rate is constant, eq. 26 can be obtained.

$$JVdt = \tfrac{JV}{q} d\Delta T = \tfrac{JV}{q}\, d\, \Delta T \qquad (26)$$

The probability of nucleation occurring in a sample of volume V at a temperature increase of $d\Delta T$ can be calculated as the product of the probability of nucleation and the probability of a sample not having nuclei at ΔT, as is shown in eq. 27. Integration of dP results in eq. 28.

$$dP = (1 - P)\left(\frac{JV}{q}\right) d\, \Delta T \qquad (27)$$

$$P = 1 - \exp\left(-\frac{k'V \cdot \Delta T^{n+1}}{q \cdot (n+1)}\right) \qquad (28)$$

MZW results are distributed around an average value ($T_{\max}$), which can be found in eq. 29.

$$\Gamma(x) = \int_0^{\inf} t^{x-1} \exp(-t)\, d\, t,$$

$$\Delta T_{\max} = \frac{\int_0^{inf} \Delta T\, dP}{d\Delta T} d\Delta T = \Gamma\left(\frac{n+2}{n+1}\right) \cdot \left(\frac{q(n+1)}{k'V}\right)^{\frac{1}{n+1}} \qquad (29)$$

Taking the logarithm of both sides results in the final eq. 30, which can be used to find the nucleation rate and order.

$$\log(\Delta T_{\max}) = \log\left(\Gamma\left(\frac{n+2}{n+1}\right)\right) + \frac{1}{n+1}\log\left(\frac{n+1}{k'V}\right) + \frac{1}{n+1}\log(q) \qquad (30)$$

Advantages: (i) To our knowledge, this is the only method that is commonly used for large volume batch crystallizers that takes into account the stochastic nature of nucleation. **(ii)** The power law can be used to describe not only homogeneous, but also secondary or heterogeneous nucleation.

Disadvantages: (i) Kubota uses an empirical power law: neither the nucleation order, nor the rate are physically sensible. They are the same parameters as in Kubota's deterministic model. **(ii)** The model does not take into account depletion of the supersaturation due to growth. **(iii)** In eq. 15 a linear solubility-temperature relationship is assumed. **(iv)** The method requires more computational effort than Kubota's deterministic model.

Sangwal's self-consistent Nývlt-like equation

Sangwal derives a Nývlt-like equation with the nucleation rate in number basis, and with a nucleation rate constant and order with physical significance[19]. He assumes that close to the MZW the nucleation rate is given as the power law shown in eq. 31[19].

$$J = k \cdot \ln^{\text{n}}(S) \qquad (31)$$

Sangwal shows that the nucleation order n is related to the dimensionless nucleation rate (J/A), interfacial energy γ and the supersaturation $\ln(S)$[19]. A small nucleation order n (*e.g.* 2-5) indicates that the solubility of the solute in the solvent is high and that stable nuclei are formed easily, more so at high solute concentrations[19]. This is explained by the aggregation of the solute molecules into nuclei clusters by diffusion in the solution. A large n (*e.g.* 20) indicates that the solubility is low and formation of stable nuclei is more difficult[19]. For nucleation of low soluble solutes the crystallizing molecules are far from each other and surrounded by solvent molecules. This results in a low probability of intermolecular collisions. The nucleation rate constant (k) is shown to decrease for increasing supersaturation values and to increase for increasing nucleation rate order[19]. This parameter is related to the formation of stable nuclei per volume per time[19].

Sangwal proposes a self-consistent Nývlt-like equation that links the dimensionless MZW (the MZW divided by saturation temperature T_0) and the cooling rate[19]. It is assumed that near the MZW, the nucleation rate is proportional to the rate of dimensionless concentration difference change ($\Delta c/c_1 \cdot \Delta t$), with f_c a constant (number of 'entities' per volume), and $c_{\text{eq},1}$ the solubility concentration at temperature T_1, as is shown in eq. 32.

$$J = f_c \frac{\Delta c}{c_1 \Delta t} = \frac{f_c \Delta c}{c_1 \Delta T} \cdot \frac{\Delta T}{\Delta t} \qquad (32)$$

The theory of regular solutions is used to explain the temperature dependency of the solubility, with ΔH_s the heat of dissolution and R_G the gas constant. Temperature T_1 is assumed to be lower than temperature T_0. This results in eq. 33. Substitution of eq. 33 in eq. 32 results in eq. 34.

$$\frac{c_0}{c_1} = \exp\left(\frac{\Delta H_s}{R_G T_1}\frac{\Delta T}{T_0}\right) \tag{33}$$

$$J = \frac{f_c \Delta c}{c_1 \Delta T}\cdot\frac{\Delta T}{\Delta t} = \frac{f_c \Delta H_s}{R_G T_1}\cdot\left(\frac{q}{T_0}\right) \tag{34}$$

Temperature T_1 in eq. 34 can be replaced by T_{det}, the temperature at which crystals are detected. The equation that follows from the theory of regular solutions can be inserted into the power law (with the temperature difference between T_0 and T_{det} being the MZW), which results in eq. 35.

$$J = k\left(\frac{\Delta H_s}{R_G T_{\mathrm{det}}}\cdot\frac{\Delta T_{\mathrm{MZW}}}{T_0}\right)^n \tag{35}$$

Substituting eq. 34 in eq. 35 and taking the logarithm results in eq. 36[19], which can be rewritten as shown in eq. 37[19]. The plot of $\log(\Delta T_{\mathrm{max}}/T_0)$ against $\log(q)$, gives ϕ as the intercept and $1/n$ as the slope.

$$\ln\left(\frac{\Delta T_{\mathrm{max}}}{T_0}\right) = \frac{1-n}{n}\cdot\ln\left(\frac{\Delta H_s}{R_G T_{\mathrm{Lim}}}\right) + \frac{1}{n}\cdot\ln\left(\frac{f_c}{k}\right) - \frac{1}{n}\cdot\ln(T_0) + \frac{1}{n}\cdot\ln(q) \tag{36}$$

$$\ln\left(\frac{\Delta T_{\mathrm{max}}}{T_0}\right) = \phi + \frac{1}{n}\cdot\ln(q) \tag{37}$$

Advantages: (i) Both nucleation rate and order have physical significance. **(ii)** Sangwal's equation is still simple to use, whilst solving some drawbacks from Nývlt's equation. **(iii)** The assumption of a linear solubility-temperature relationship can be avoided by using the theory of regular solutions. The method does require solubility data (ΔH_S). **Disadvantages: (i)** Sangwal assumes a power law for the nucleation rate (eq. 31). In eq. 32 it is assumed that the nucleation rate is equal to the product of the dimensionless concentration difference generation and the number of entities. **(ii)** The growth of crystals and depletion of the supersaturation due to growth was not taken into account in this approach. **(iii)** Sangwal has shown that the values of ϕ and n are not sensitive to the detection method, by comparing the detection via the ultrasound technique and detection based on the appearance of visible crystals[19]. Nevertheless, the detection method is not taken into account. **(iv)** To our knowledge, not a lot of other authors have applied Sangwal's method, possibly due to the lack of applicability and advantages over other models. This makes comparisons for different systems difficult. **(v)** The definition of f_c (as number of entities) is difficult to know as long as the presence of mesoscale clusters and their abundancy remains unknown. Sangwal proposes a constant value $f_c \approx 10^{29}$molecules·m^{-3} as an upper limit[19].

In another paper, Sangwal abandons the Nývlt and power law approach, which leads to a linear dependency of the (dimensionless) MZW and cooling rate, and proposes a new model based on the CNT[20]. Both models result in different predictions. This second model results in eq. 38 [20]:

$$\left(\frac{\Delta T_{\mathrm{MZW}}}{T_0}\right)^{-2} = F_1\cdot\left[\ln\left(\frac{A}{F_1}\frac{R_G T_{\mathrm{Lim}}}{\Delta H_s}\right) + \ln(T_0)\right] - F_1\cdot\ln(q) \tag{38},$$

$$\text{with } F_1 = \left[\frac{3}{16\pi}\left(\frac{k\,T_{\mathrm{Lim}}}{\gamma v^{\frac{2}{3}}}\right)^3\cdot\left(\frac{\Delta H_s}{R_G T_{\mathrm{Lim}}}\right)^2\right]$$

Kim and Mersmann, Mersmann and Bartosch approaches

Kim and Mersmann have developed a model to relate the MZW to the dominating nucleation mechanism[81]. They first give an equation for the homogeneous and heterogeneous nucleation (as shown in Table 3)[80,81,90], with f_M a reduction factor (0.1-1), φ_{HE} the heterogeneity factor (10^{-11}), φ_{M} the volumetric hold up of crystals, D_{AB} the diffusion coefficient, c_c the molar density of the crystal (usually 5-40 kmol/m^3), N_A Avogadro number, d_m the molecule diameter and A_c the crystal surface. For homogeneous nucleation both the heterogeneity factor and the reduction factor are unity[82]. Mersmann and Bartosch's theoretical model to predict the MZW assumes surface nucleation is the decisive mechanism before the detection of crystals in large volume crystallizers[80]. The surface nucleation equation is based on a model by Nielsen (also shown in Table 3)[90,91]. For surface nucleation E is the efficiency factor (0-1) to account for the fact that not all surface nuclei become nuclei in the bulk solution. The total rate of nucleation can be found by summing all the contributions together, as shown in eq. 39.

$$J = J_{\mathrm{HO}} + J_{\mathrm{HE}} + J_{\mathrm{sur}} + J_{\mathrm{att}} \tag{39}$$

Table 3 Formulas for different nucleation mechanisms as given by Mersmann *et al.*

Nucleation mechanism	Theoretical nucleation equations[80,81,90]
Homogeneous	$J_{\mathrm{HO}} = 0.965 \cdot D_{AB}(N_A c_c)^{\frac{5}{3}} \left(\frac{c_{\mathrm{eq}}}{\rho_c}\right)^{\frac{7}{3}} S^{\frac{7}{3}} \cdot \sqrt{\ln\left(\frac{c_c}{c_{\mathrm{eq}}}\right)} \cdot \exp\left[-\frac{1.19 \ln\left(\frac{c_c}{c_{\mathrm{eq}}}\right)^3}{\ln(S)^2}\right]$
Heterogeneous	$J_{\mathrm{HE}} = 0.965 \cdot \varphi_{\mathrm{HE}} D_{AB}(N_A c_c)^{\frac{5}{3}} \left(\frac{c_{\mathrm{eq}}}{\rho_c}\right)^{\frac{7}{3}} S^{\frac{7}{3}} \cdot \sqrt{f_M \ln\left(\frac{c_c}{c_{\mathrm{eq}}}\right)} \cdot \exp\left[-\frac{1.19 f_M \ln\left(\frac{c_c}{c_{\mathrm{eq}}}\right)^3}{\ln(S)^2}\right]$
Surface	$J_{\mathrm{surf}} = E A_c \cdot \frac{D_{AB}}{d_m^4} \cdot \exp\left[-\frac{\pi}{9} \frac{\ln\left(\frac{c_c}{c_{\mathrm{eq}}}\right)^2}{\ln\left(1 + \Delta c / c_{\mathrm{eq}}\right)}\right]$

The MZW and the maximum concentration difference are related, as shown in eq. 40. Kim and Mersmann then relate the time (t_{end}) required for the first crystals to be detected, to the maximum concentration difference, as shown in eq. 41.

$$\Delta T_{\max} = \frac{T}{c_{eq}} \frac{d \ln(T)}{d \ln\left(c_{\mathrm{eq}}\right)} \cdot \Delta c_{\max} \tag{40}$$

$$t_{\mathrm{det}} = \frac{\Delta T_{\max}}{q} = \frac{\Delta c_{\max}}{c_{\mathrm{eq}}} \cdot \frac{d \ln(T)\, T}{d \ln\left(c_{\mathrm{eq}}\right) q} \tag{41}$$

Kim and Mersmann assume that the supersaturation increases proportionally with the supersaturation rate, which is expressed as the nucleation rate in mass basis, with $\Delta\rho$ the mass-based supersaturation, as shown in eq. 42[81]. At $t = t_{\mathrm{end}}$ the maximum value is obtained. Similarly as Nývlt, the mass based nucleation rate is related to the supersaturation rate, as shown in eq. 43.

$$J_m = \frac{\Delta\rho}{t} \tag{42}$$

$$J_m = k_m \Delta\rho_{\max}^n \tag{43}$$

The number of crystals can then be calculated by transforming the nucleation rate in number basis ($J = dN/dt$) to the mass based nucleation rate as defined by Nývlt, with k_v the volume shape factor, with c_c the crystal molar density, as shown in eq. 44.

$$N = \int_0^{t_{\mathrm{det}}} \frac{dN}{dt} dt = \int_0^{t_{\mathrm{det}}} k_m \frac{\Delta\rho^n}{k_v c_c r_{\mathrm{det}}^3} dt = \frac{\Delta c_{\max}}{(n+1) k_v c_c r_{\mathrm{det}}^3} \tag{44}$$

The total primary nucleation rate is approximated at the point of detection, as shown in eq. 45.

$$J = \frac{\mathrm{N}}{\mathrm{t_{end}}} \tag{45}$$

Solving one of the equations (Table 3, eq. 41, eq. 44 and eq. 45**)** results in f_M the reduction factor, φ_{HE} the heterogeneity factor (10^{-11}) and n the nucleation rate order. For each equation in Table 3, the equations are combined, which results in the equations shown in Table 4.

Table 4 Theoretical models for the calculation of the MZW, from Mersmann *et al.*

Nucleation mechanism	Theoretical equations for predicting the MZW[80,81,90]
Homogeneous	$\frac{c[d(\ln c_{\mathrm{eq}})/d(\ln T)]\, T}{0.965(n+1) r_{\mathrm{det}}^3 k_v c_c T D_{AB}(N_A c_c)^{\frac{5}{3}} \left(\frac{c_{\max,\mathrm{eq}}}{c_c}\right)^{\frac{7}{3}} \cdot \left(\ln\left(\frac{c_c}{c_{\max,\mathrm{eq}}}\right)\right)^{\frac{1}{2}}} = S_{\max,\mathrm{hom}}^{7/3} \cdot \exp\left[-1.19 \left(\ln\left(\frac{c_c}{c_{\max,\mathrm{eq}}}\right)^3 \left(\ln\left(S_{\max,\mathrm{hom}}\right)\right)^{-2}\right]\right.$

Heterogeneous	$\frac{c[d(\ln c_{\mathrm{eq}})/d(\ln T)]\,T}{0.965(n+1)r_{\mathrm{det}}^3 k_v c_c T D_{AB}\varphi_M (N_A c_c)^{\frac{5}{3}}\left(\frac{c_{\mathrm{max,eq}}}{c_c}\right)^{\frac{7}{3}}\left(\ln\left(\frac{c_c}{c_{\mathrm{max,eq}}}\right)\right)^{\frac{1}{2}}} = S_{\mathrm{max,hom}}^{7/3}\sqrt{f_M \ln(c_c/c_{\mathrm{met}}^*)}\cdot\exp[-1.19 f_M(\ln\left(\frac{c_c}{c_{\mathrm{max,eq}}}\right)^3\left(\ln(S_{\mathrm{max,hom}})\right)^{-2}]$
Surface	$S_{\mathrm{max,surf}} = \exp\left[\left(-\frac{9}{\pi\left(\ln\left(\frac{c_c}{c_{\mathrm{max,eq}}}\right)^2\right)}\ln\left[c_{\mathrm{max,eq}}\frac{\left(\frac{d\ln(c_{\mathrm{eq}})}{d\ln(T)}\right)q\, d_m^{-4}}{6E\varphi_M D_{AB}(n+1)k_v c_c r_{\mathrm{det}}^3 T}\right]\right)^{-1}\right]$

Advantages: (i) The reduction factor gives information about the nucleation mechanism. Heterogeneous nucleation is expected for small reduction factors. **(ii)** If seed crystals are present, surface nucleation is assumed to be the dominating mechanism. The model can thus be applied for seeded batch crystallization processes. **(iii)** A more simplified model is available (in ref.[80]). **(iv)** The method takes crystal detection into account, via the volumetric holdup parameter. For detection with a light beam, 10^{-3}-10^{-4} can be used[80]. **Disadvantages: (i)** It is a complex model, which requires significant computational effort. A lot of parameters are required: $D_{AB}, c_c, d\ln(c_{\mathrm{eq}})/d\ln(T)$. Also, the radius of detectable crystals (r_{det}) must be known to transform the mass based nucleation rate into the number based one. **(ii)** The method assumes constant $d\ln(c_{\mathrm{eq}})/dt$. Also, eq. 42 relies on an assumption and eq. 40 is only valid for $\Delta c/c_{\mathrm{eq}} < 0.5$ [80]. **(iii)** Eq. 44 overestimates the nucleation rate by assuming the nucleation rate at the high supersaturation (right at the moment of detection) is the nucleation rate for the entire process. In reality the nucleation rate starts low and increases during polythermal measurements. **(iv)** Multiple datasets are required to find all parameters. **(v)** Mersmann *et al.* also assume that there is no depletion of the supersaturation due to crystal growth[80].

KBHR model

Kashchiev *et al*. starts from the Kolmogorov-Johonson-Mehl-Avrami (KJMA) method[22,26,92]. The KBHR approach assumes that the PNM is correct. A further division is made between "instantaneous (IN)" and "progressive (PN)" nucleation. For IN all nuclei nucleate at the same time, *e.g.* due to the presence of a lot of heterogeneous nucleation sites or secondary nucleation from a few parent or seed crystals[92]. For PN, nuclei nucleate at different times. Depending on the mechanism involved, the obtained nucleation rates are different – which in turn results in different $\ln(\Delta T_{\mathrm{max}})$ versus $\ln(q)$ formulas. Nucleation is detected either when a certain fraction of the solution volume contains crystals ($\alpha_{\mathrm{det}} = V_c/V$, with V_c the crystalline volume) or when a large number of crystals is present in the solution (N_{det}). The authors acknowledge that the growth rate also determines these values. The KJMA formula for the volume fraction of crystals as a function of time (for $\alpha < 0.1$) is given by eq. 46[26], with J the heterogeneous and homogeneous nucleation rate, G [m/s] the time-dependent linear growth rate, d the dimensionality of the crystal growth and $k_v[m^{3-d}]$ the growth shape factor[22]. N is the total amount of crystals nucleated in volume V and time t, as is shown in eq. 47. It is assumed that the crystals are growing in a solution with volume V and are not in contact with each other (which is only true for the beginning of nucleation)[26]. The shape factors can be found in the book by Kashchiev, ref. [26]. Also, an isothermal KBHR method is discussed which is out of scope for this text[21]. A flow chart of the complete KBHR approach can be found in the paper by Camacho Corzo *et al.*[21].

$$\alpha(t) = k_v \int_0^t J(t')\left[\int_0^{t-t'} G(t")\,dt"\right]^{d_g} dt' \quad (46)$$

$$N = V\int_0^t J(t')dt' \quad (47)$$

The MZW is non-dimensionalized by dividing it by the equilibrium temperature, this quantity is called the critical undercooling u_c, as shown in eq. 48. The growth rate (m/s) is assumed as shown in eq. 49, with n_g and m_g (0.5-1) the growth rate parameters, k_g the growth rate constant[22].

$$u_c = \frac{\Delta T_{\mathrm{max}}}{T_{\mathrm{eq}}} = \frac{q\cdot t_{\mathrm{max}}}{T_{\mathrm{eq}}} \quad (48)$$

$$G(t) = m_g\left(\frac{T_{\mathrm{eq}}}{q}\right)^{m_g-1}\cdot k_g^m\cdot\left[1-\exp\left(\frac{-au}{1-u}\right)\right]^{n_g m_g}\cdot u^{m_g-1},$$

$$J = A\exp\left(-\frac{b}{(1-u)\cdot u^2}\right)$$

(49)

Eq. 48 can be expressed in terms of undercooling. This equation has an analytical solution (which is different for IN and PN) if the equalities $u_c < 0.1, au_c < 1$ are met[21]. Otherwise it must be solved numerically[21]. To distinguish between PN and IN the 'rule of three' is used: the slope of a plot of u_c versus q is less than three in the IN case, and greater than three in the PN case[21].

PN-case (discussed in ref.[22]): if the equalities $u_c < 0.1, au_c < 1$ are met, with $a = \zeta/k_bT_c$ the dimensionless latent heat of crystallization and k_b the Boltzmann constant. If the number of crystals N_{det} is used to detect the onset of nucleation, eq. 50 is obtained. A is the nucleation rate constant and b is the dimensionalized thermodynamic parameter $\frac{16\cdot\pi\nu^2\gamma^3}{3\cdot k_bT\zeta^2}$, with ζ the molecular latent heat of the crystallization process and ν the molecular volume. If the fraction α_{det} is used to determine the onset of crystallization a different formula is obtained, for which we refer to ref.[22].

$$\ln(q) = \ln\left(\frac{VA\cdot T_{\mathrm{eq}}}{N_{\mathrm{det}}2b}\right) + 3\ln(u_c) - \frac{b}{(1-u_c)\cdot u_c^2} \quad (50)$$

IN-case (discussed in ref.[92]): if the equalities $u_c < 0.1, au_c < 1$ are met and the IN-case can be applied (all crystals appear at the same moment with concentration c_0 at the moment t_0 at a dimensionless undercooling of u_0). For IN all crystals are growing to a detectable size at the same time. After nucleation the number of crystals is constant and all crystals have the same size[92]. In this case, eq. 51 and eq. 52 are obtained[92]. q_0 takes into account both growth and nucleation. No nucleation parameters remain in the equation apart from the detectable crystal volume fraction and the concentration of crystals at nucleation. d_g in eq. 52 is the growth dimensionality parameter.

$$\ln(q) = \ln(q_0) + \frac{1}{m_g}\cdot\ln\left[u_c^{(n_g+1)m_g} - u_0^{(n_g+1)m_g}\right] \quad (51)$$

$$q_0 = \left[\frac{k_v c_0}{(n_g+1)^{d_g}\alpha_{\mathrm{det}}}\right]^{\frac{1}{m_g d_g}} a^{n_g} k_g T_{\mathrm{eq}} \quad (52)$$

Advantages: (i) The KBHR model allows fast characterization of the mechanism of nucleation (IN- or PN-ruled via the rule of three) and **(ii)** takes into account both nucleation and growth of crystals based on this mechanism. **(iii)** The model avoids the (semi-)empirical equations for the nucleation rate. **(iv)** The nucleation parameters have physical meaning. **(v)** The model takes into account how the detection of the onset of crystallization is measured (N_{det} or α_{det}). **(vi)** Kashchiev and colleagues also give a (linear) Nývlt-like equation which is applicable if certain inequalities are met[22,92]. **(vii)** There is also an isothermal method which can be used as a check. **Disadvantages: (i)** Eq. 51 is sensitive to the available data which may lead to physically impossible values for the parameters[92]. **(ii)** If the inequalities $u_c < 0.1, au_c < 1$ are not met, equation 46 must be solved numerically, which is computationally difficult. **(iii)** For the IN-case, no nucleation data is obtained. **(iv)** Eq. 51 is used for the growth rate, which assumes k_G constant, which is unreasonable for crystallite growth by two-dimensional nucleation[22]. **(v)** The model is quite complex and requires some effort.

Kashchiev *et al.* induction time model

Kashchiev *et al.* also proposed a general formula for the induction time, which is applicable for time independent nucleation rates[37]. Kashchiev makes the distinction between the MNM and the PNM, resulting in different expressions for the induction time.

MNM: the metastability of the system is lost once the first nucleus is formed. The induction time can then be calculated easily $t_i = 1/JV$. As the growth time is assumed to be zero, the detection of an extremely small nucleus is required (10-1000 molecules)[37]. This must be taken into account when using this formula. Further it must be noted that the induction time mentioned here is the mean time for the appearance of a first nucleus[37].

PNM: multiple nuclei can be formed, while the first critical nuclei grow to a detectable size. Kashchiev derives the formula: $t_i = (4\alpha/k_vJG^3)^{1/4}$, with $\alpha = V_m/V \leq 1$ and V_m the volume of a detectable nucleus and k_v a shape factor[37]. This formula takes (3D) growth of the crystal nuclei into account. The dependence of V is lost in the PNM approach.

Kashchiev *et al.* also propose a general approach for the induction time: $t_{\mathrm{ind}} = t_{MNM} + t_{PN}$, which results in eq. 53[37]. Kashchiev *et al.*'s approach does not include a relaxation time, the time required for the system to achieve a "quasi-steady-state distribution of molecular clusters", like Mullin proposes[23].

$$t_i = \frac{1}{JV} + \left(\frac{4\alpha}{k_vJG^3}\right)^{\frac{1}{4}} \quad (53)$$

Advantages: (i) A general formula is proposed which unifies the IN and PN approach. **(ii)** Takes into account the volume of detectable nuclei for PNM. **(iii)** Kashchiev and his colleagues generalized eq. 53 for 1D, 2D and 3D growth (volume diffusion controlled growth, surface controlled growth)[37]. **(iv)** The CNT nucleation rate can be used in formula eq. 53. **Disadvantages: (i)** The PNM equation assumes constant nucleation and 3D growth rates[37]. It is valid for the region where nucleation-mediated growth of crystals (2D) occurs[37]. **(ii)** In the general formula it is assumed that 2D induction time principles can be adapted to 3D nucleation and growth.

Nagy *et al.* method

We also briefly discuss Nagy *et al.*'s PBE method as it results in an Nývlt-like equation. Nagy's approach uses population balance equations and the conservation of mass to quantify both nucleation and growth rates[82]. The nucleation rate (in number basis) and the growth rate are defined as power laws as shown in eq. 54.

$$G = k_g \Delta c^g, \;\; J = k \Delta c^n \tag{54}$$

The goal is to determine the parameters k_g, g, k, n. Solving the PBEs results in the crystal size distribution ($f_n(L,t)$), with L the characteristic size of the crystals and f_n the crystal population density, which is the number of crystals per unit size per unit volume[23]. A PBE tracks the number density and how crystal properties change[93]. The moment method is an efficient (from the computational point of view) method for solving PBEs. Moments are defined as shown in eq. 55.

$$\mu_j = \int_0^{\inf} L^j f_n(L,t)\, dL \tag{55}$$

The j^{th} moment with j equal to 0 (zeroth moment), 1 (first moment), 2 (second moment), 3 (third moment) respectively correspond to: the total number, the cumulative length, the surface area, and the volume of all crystals. The conservation of mass equation can be formulated as shown in eq. 56, with k_v the volume shape factor, M the mass of crystals and ρ the density of a crystal.

$$dM = f_n L^3 k_v \rho dL \tag{56}$$

By taking the derivative of the moments, the matrix in eq. 57 can be constructed, with r_{crit} as the size of a nuclei and c the solution concentration. The experimental CSD is then fitted to the theoretical model, to obtain the nucleation and growth rate and order. The rate of cooling is taken into account indirectly through the size of the particles. Nagy *et al.* demonstrates this by using a nonlinear least-squares programming technique[82].

$$\begin{bmatrix} \dot{\mu_0} \\ \dot{\mu_1} \\ \dot{\mu_2} \\ \dot{\mu_3} \\ \dot{c} \end{bmatrix} = \begin{bmatrix} J \\ G\mu_0 + J\, r_{\text{crit}} \\ 2G\mu_1 + J\, r_{\text{crit}} \\ 3G\mu_2 + J\, r_{\text{crit}}^3 \\ -\rho_c k_v \left(3G\mu_2 + J\, r_{\text{crit}}^3\right) \end{bmatrix} \tag{57}$$

Nagy *et al.* derive an expression similar to the Nývlt equation, by assuming crystals nucleate at a critical size $r_{\text{crit}} = 0$ at time t and then continue to grow to a detectable size with the growth kinetics[82]. This equation is shown in eq. 58, with $m = (3g + n + 4)/4$ the "apparent nucleation rate order", constant K contains the shape factor, the growth order, the nucleation order and other parameters. The complete derivation of the formula can be found in their paper[82]. This Nývlt-like equation from Nagy *et al*. results in the same slope for log(q) versus $\log(\Delta T_{\text{max}})$ as the Söhnel and Nývlt model for detection based on the cloud of crystals, and the Hulbert model[76,87].

$$\ln(q) = (m-1) \cdot \ln\left(\frac{dc_{\text{eq}}}{dT}\right) + \ln(K) + m \cdot \ln(\Delta T_{\text{max}}) \tag{58}$$

Advantages: (i) Simultaneous determination of growth and nucleation kinetics. **(ii)** The model is more complex but an analogy to the easy-to-use Nývlt approach is proposed (assuming constant $\ln(dc_{\text{eq}}/dT)$. **(iii)** Seeding can be taking into account by changing the model boundary conditions. The empirical power law might not describe secondary nucleation accurately though. **(iv)** Nagy *et al*. compared their approach to the classical Nývlt and Kim and Mersmann approaches[82]. **Disadvantages: (i)** The model uses empirical power law equations for both nucleation and growth, which does not give information about the mechanisms of nucleation and results in parameters without any physical significance. **(ii)** Requires more experimental data (CSD and solution concentration) and additional computational effort than standard isothermal and polythermal data analysis models.

Other methods

For completeness we also mention some other approaches. Harano *et al.* have proposed an isothermal data analysis method to determine nucleation kinetics[77]. Harano *et al.* propose a

nucleation rate expression based on the CNT, shown in eq. 59, with k a constant and n the amount of solute molecules present in a critical nucleus, which is dependent on the supersaturation[77]. Harano *et al.*'s method, which is shown in eq. 60, takes into account the detection method. Similarly, also a polythermal method was proposed[79].

$$J = k\,S^n, \quad k = k_2 \cdot \exp\left(-\frac{4\pi \cdot r_{crit}^2 \cdot \gamma}{k_b \cdot T}\right) \qquad (59)$$

$$\log(t_{\mathrm{det}}) = \log\left(\frac{N_{\mathrm{det}}}{V}\right) - \log(J) \qquad (60)$$

Preckshot *et al.* proposed an equation similar to that of Harano *et al.* Preckshot *et al.*'s equation is shown in eq. 61[75,77,78].

$$\log(t_{\mathrm{det}}V) = -\log\left(\frac{k}{N_{\mathrm{det}}}\right) + M_P \cdot \log^{-2}(S),$$
$$M_P = \frac{16}{3}\pi \cdot \left(\frac{\sigma}{2.303 \cdot kT}\right)^3 \nu^2 \qquad (61)$$

Shiau and Lu have developed isothermal and polythermal data analysis methods for PN, that can be applied if turbidity is used to detect the onset of crystallization[83,84]. The CNT nucleation rate is related to the induction time and MZW[84]. Three different cases are discussed: detection based on the minimum area density [m^2m^{-3}], on the minimum number density [m^{-3}], or on the minimum detectable volume fraction [-] required for detection of crystals[83]. It is assumed that crystals nucleate at size 0[83]. Growth of the crystals is taken into account, but not the supersaturation depletion due to growth[83]. In 2019, Shiau has proposed another isothermal data analysis method, to study the influence of different solvents on the nucleation kinetics, by splitting the nucleation rate into an intrinsic kinetic parameter and a part dependent on the interfacial energy[94].

Dugua and Simon (1978) proposed to extract the nucleation rate from isothermal measurements, based on the amount of crystallized mass $M(t)$ formed[95]. The amount of mass precipitation in a time t from crystals nucleated at time t_0 can be calculated as shown in eq. 62, with $m(t_0)$ the mass of a crystal at time t that has nucleated at time t_0:

$$dM(t) = J(t_0) \cdot dt_0 \cdot V(t_0) \cdot m(t - t_0) \qquad (62)$$

By assuming all crystals have the same $m(t)$, for isothermal measurements, the total mass at time t can be calculated[95]. If the function $m(t)$ is known, the nucleation rate can be found by deconvoluting eq. 63 [95].

$$M(t) = \int_0^t J(t_0) \cdot V(t_0) \cdot m(t - t_0)\, dt_0 \qquad (63)$$

Boistelle and Astier (1988) proposed plotting the induction time versus $\log^{-2}(S)$, such that the nucleation parameters can be determined, by assuming that at the induction time one nucleus per unit volume has formed[96]. Kobari and Kubota have tried to construct a more unified approach by using PBEs and the formulas from Kubota's models[13]. Mutaftschiev and Platikanova (1961) decided to simply count the crystals flowing in solution[95].

PART II: MICROFLUIDIC AND MICROVIAL CRYSTALLIZERS

Microfluidic and microvial crystallizers are miniaturized crystallizers. Their characteristic small volume makes them an excellent tool for crystallization research, due to the many advantages over large volume crystallizers[97–99]. The high surface-to-volume ratios result in high mass and heat transfer rates, which allows for good control over the experimental conditions (*e.g.* extremely high supersaturations). They are used to do high-throughput screening, with low material consumption, and to obtain fundamental insights into the mechanism of nucleation[2,45,66,97,100–103]. In small volumes the observation zone for nucleation detection is reduced significantly, which results in more accurate crystal detection[67]. Another advantage is that impurities that act as heterogeneous nucleation sites can be removed more easily. We make the distinction between high-throughput microfluidic crystallizers (<1mL) and medium-throughput "microvial" crystallizers, that are slightly larger (1-10mL) but offer similar advantages although to a lesser extent. Table 5 gives an overview of all the microvial and microfluidic methods discussed in **Part II.**

Table 5 Microvial and microfluidic discussed in Part II of this review and the page number where these methods are discussed in this review.

Microvial and Microfluidic methods	Pg.
Double-pulse technique	15
Isothermal (stagnant) droplet technique	15
Droplet technique in flow	16
Time-varying supersaturation droplet technique	17
Isothermal microvial technique	19
Polythermal microvial technique	20
Other microvial techniques	20

Double-pulse technique

The double-pulse technique aims to decouple nucleation from the ensuing crystals growth[62,104]. This can be done in well-controlled environments

like microcrystallizers and droplets by manipulating the temperature. The technique was independently proposed in 1999 by Galkin and Vekilov, and by Tsekova *et al.*[34,105]. Nucleation usually only occurs at higher supersaturations, for which growth is very fast. This leads to a depletion of the supersaturation by growth and complicates the nucleation rate measurements. To solve this problem the solution is first kept at a high supersaturation until nucleation occurs. Then, the supersaturation is lowered (into the MZW), such that the existing nuclei can grow to a detectable size without nucleation of other crystals. Galkin and Vekilov propose to put the temperature of the growth zone close to the solubility curve, to suppress nucleation[105]. The double-pulse technique is graphically explained in Figure 5. The double-pulse technique has contributed to the discovery of the two-step nucleation mechanism[1,33]. The double-pulse technique is presented here as a microfluidic (droplet) technique, but is in principle also applicable in slightly larger volumes: *e.g.* Nanev *et al.* used the technique for insulin crystallization in a small well[106].

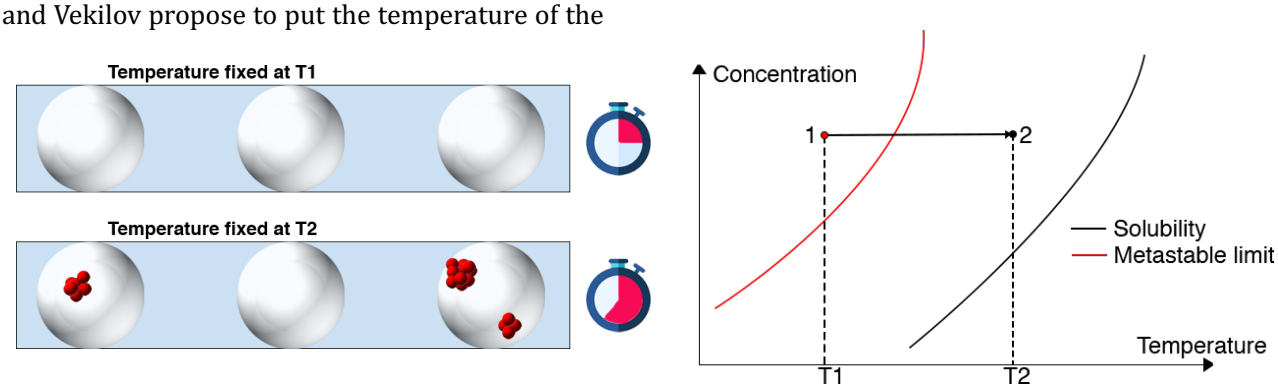

(a) (b)

Figure 5 (a) Graphical representation of the double-pulse technique for droplets. **(b)** The double-pulse technique illustrated on the phase diagram: first the nucleation step is performed (indicated by point 1), then the growth step (indicated by point 2), after Ildefonso *et al.*[107].

Advantages: (i) The main advantage is the "decoupling" of nucleation and growth. The majority of the supersaturation depletion is in the growth stage. Thus, the assumption for isothermal measurements that the supersaturation is constant throughout the entire experiment is reasonably valid. **(ii)** The technique can be (and often is) combined with other techniques (*e.g.* the droplet technique). **Disadvantages: (i)** The decoupling technique requires prior knowledge of the Miers' phase diagram. **(ii)** The time duration for which the solution is kept in the nucleation zone affects the results. **(iii)** It is impossible to know that crystals detected in the growth zone did not nucleate in the growth zone (even though the probability of nucleation is lower). The supersaturation may still be sufficiently high for heterogeneous or secondary nucleation. **(iv)** The CNT predicts that the critical size is inversely proportional to the temperature difference between the temperature of the solution and the solubility temperature. Crystals nucleating at size r_{crit} in the nucleation zone, may dissolve in the growth zone because the critical size required in the growth zone (which is at lower temperature) is higher[108]. Thus, crystals need to grow slightly in the nucleation zone or crystals nucleated in the nucleation zone are dissolved in the growth zone. **(v)** The technique can be time-consuming[106].

Lounaci *et al.* have shown that crystallization of lysozyme in microcrystallizers is dependent on the channel height (18-150μm): deeper channels favor nucleation, shallow channels favor growth[109]. They propose a decoupling strategy based on sections of different channel heights, rather than different temperatures[109].

Isothermal droplet technique

One of the most used techniques for nucleation rate estimation is the (isothermal) droplet technique, which is based on Turnbull and Vonnegut's research concerning supercooled metallic droplets[110,111]. In the droplet technique a supersatured liquid is confined in a number of droplets in an immiscible carrier fluid. The droplet technique is generally performed in easy-to-use microfluidic platforms, fabricated by lithography[112,113]. Droplet microfluidics offer similar advantages to microcrystallizers, whilst reducing clogging and overcoming Taylor dispersion[113]. The distinction is generally made between droplet generation (dominated by the confinement and the interfacial forces) and droplet

storage. An example of crystals in a droplet is shown Figure 6. A complete overview of droplet generation can be found in the paper by Zhu *et al.*[114].

In the droplet technique each individual droplet is considered as a distinct "batch crystallizer". Hence, a lot of different conditions can be tested in a short time with minimal material consumption. Droplets of varying volumes (from nL to μL droplets) are generated with emulsion-based methods (high-throughput generation)[115]. For even smaller volumes (pL-fL) microinjection is used (generally low-throughput generation)[67,115]. Both stagnant and moving droplets have been used. In the conventional droplet technique, droplets are cooled to a fixed supersaturation for a fixed time t, during which nucleation takes place. The fraction of droplets containing crystals is recorded. The experimental probability (P_{exp}) is calculated by taking the ratio of droplets containing crystals (N_c) over the total amount of droplets (N), as shown in eq. 64. This experimental probability can then be fitted to theoretical probability of the MNM (eq. 12).

$$P_{\text{exp}} = \text{N}_\text{c}/N \tag{64}$$

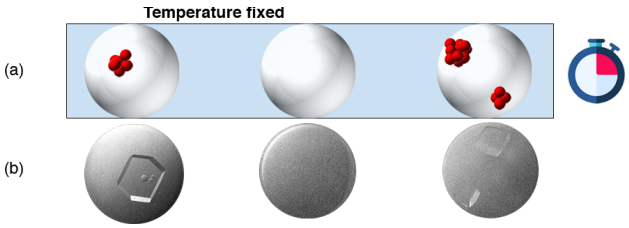

Figure 6 (a) Graphical representation of the isothermal droplet technique. **(b)** Two droplets (radius approx. 1mm) with a varying number of (lysozyme) crystals. Both droplets are kept under identical conditions, droplets cut out[34]. Reprinted with permission from J. Cryst. Growth 2001, 232, 63–76. Copyright (2001) Elsevier.

Advantages: (i) The droplet technique adheres well to the MNM technique, because of the extremely small volumes of the droplets. **(ii)** The droplet technique offers unique control over both time and space of the nucleation process[116], unmatched by any other technique. The small volume also facilitates the removal of impurities before commencement of nucleation, compared to large volume batch crystallizers. **(iii)** Large amount of data can be gathered in a short time, because each droplet is considered as an independent batch crystallizer. **(iv)** The droplet technique can be combined with the double-pulse technique. **Disadvantages: (i)** Surfactants are extensively used in the generation of droplets to stabilize and prevent coalescence[117], but might affect nucleation[101,118–120]. If no surfactants are used, heterogeneous nucleation might occur on the gas-liquid interface[121]. **(ii)** Equations from MNM are used. For these assumptions we refer to Subsection "Isothermal and Polythermal experiments". **(iii)** Experimental practicalities can cause errors: dispersing the droplets is difficult and usually the obtained droplets are not perfectly monodispersed[101,118]. Dos Santos *et al.* stress that the droplet volume distribution must be reported, as it affects the accuracy of the final results[122]. **(iii)** Because the droplets are in a carrier fluid, temperature quenches can be difficult[101]. **(iv)** The experimental operating range is limited (*e.g.* no agitation).

To measure the primary homogeneous nucleation rate, droplets must be free of impurities. This can be challenging, for example Teychené *et al.*'s results suggest that impurities at the droplet interface were still present[123]. Pound and La Mer have developed a model to find the homogeneous and heterogeneous nucleation rate using the droplet method[123–125]. A Poisson distribution is applied to the distribution of impurities in the droplets[124]. The probability that a droplet does not contain a crystal for isothermal measurements is shown in eq. 65, with m_{avg} the "arithmetic average number of active foreign nucleation sites per droplet", k_{HE} the heterogeneous nucleation rate (s^{-1}) for a single impurity in a droplet and k_{HO} (s^{-1}) the homogeneous nucleation rate[125,126]. The experimental probability curve can be found in eq. 66, with N_0 the number of drops with no crystals and N_t the total amount of droplets. This method does not distinguish between foreign particles that might be more active at lower temperatures, but assumes uniform activity for all impurities[118]. Akella *et al.* give a detailed overview of the Pound and La Mer model and its relationship to the CNT[125].

$$P_0(t) = e^{-m_{\text{avg}}}(e^{-k_{\text{HO}}t} - 1) + e^{-m_{\text{avg}}}e^{m_{\text{avg}}e^{-k_{\text{HE}}t}} \tag{65}$$

$$P_{0,\text{exp}} = \text{N}_0/N_t \tag{66}$$

Droplet technique in flow

To generate droplets for the droplet method an immiscible fluid is injected into a continuous liquid stream[114]. For the stagnant droplet method, the droplets are immobilized and supersaturation is generated. In the flowing droplet technique the flow of droplets is not stopped and droplets are generated continuously throughout the experiment. An example of a droplet microfluidic crystallizer is shown in Figure 7. As droplets flow through the microfluidic apparatus, the supersaturation is generated and the temperature

is kept constant. The probability of crystals nucleating in a droplet is recorded as a function of time. This time is defined as the distance the droplets have covered divided by their flow velocity. The degree of micromixing is affected by the flow velocity. For example Laval *et al.* (2007) used the droplet technique in flow for crystallization of potassium nitrate in water, but did not elaborate on the effects of flow ($A \approx 3 \cdot 10^7 m^{-3}s^{-1}$, $B \approx 12$)[101]. In a later paper Laval *et al.* (2009) performed similar experiments for stagnant droplets ($A \approx 1.6 \cdot 10^9 m^{-3}s^{-1}$, $B \approx 37$)[118]. Based on these results it could be concluded that droplets flowing through the microchannel reduces the nucleation rate. This is surprising, as flow increases mixing, but in both papers nucleation seems to occur via heterogeneous nucleation, which makes comparisons difficult[101,118]. Teychené *et al.* have shown that the flowing droplet technique can give both qualitative (rheological behavior, structure formation) and quantitative (nucleation rates) information[123]. A table of authors using the microfluidic droplet method is given in Table 6.

Rossi *et al.* and Nappo *et al.* applied a combination of the droplet and double-pulse technique, both for stagnant and flowing droplets[45,127]. First, droplets are stored in or flowing through the nucleation section. After a fixed (residence) time in the nucleation section, the droplets are stored in the growth section. Their results show a significantly larger nucleation rate (up to 3 orders of magnitude) for flowing droplets than for stagnant droplets. Rossi *et al.* hypothesize that the circulation patterns inside the droplets results in an increased kinetic nucleation parameter without affecting the thermodynamic nucleation parameter[45]. Nappo *et al.* conclude that the fluid-induced shear affects the nucleation process up to a certain level[127].

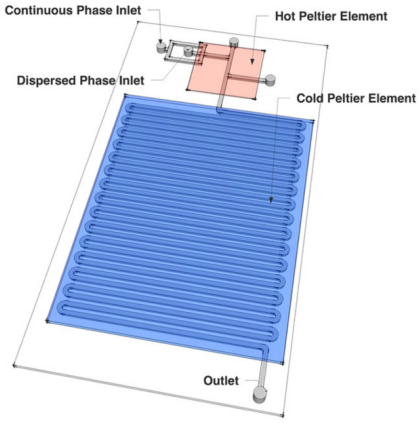

Figure 7 Example of an experimental setup for the droplet technique[116,123]. Reprinted with permission from Cryst. Growth Des. 2011, 11, 11, 4810–4818. Copyright (2011) American Chemical Society.

Advantages: (i) The flow rate can be changed and the influence of micromixing on the nucleation rate can be studied. Figure 8 shows the difference in cumulative probability for a stagnant and flowing droplet setup. Changing the flow rate may also affect the interfacial area[128]. **(ii)** For other advantages, we refer to the advantages for the stagnant droplet techniques. **Disadvantages:** The droplet technique for flowing droplets suffers from the same disadvantages as the droplet techniques for stagnant droplets. Flowing droplet experiments may also be more difficult.

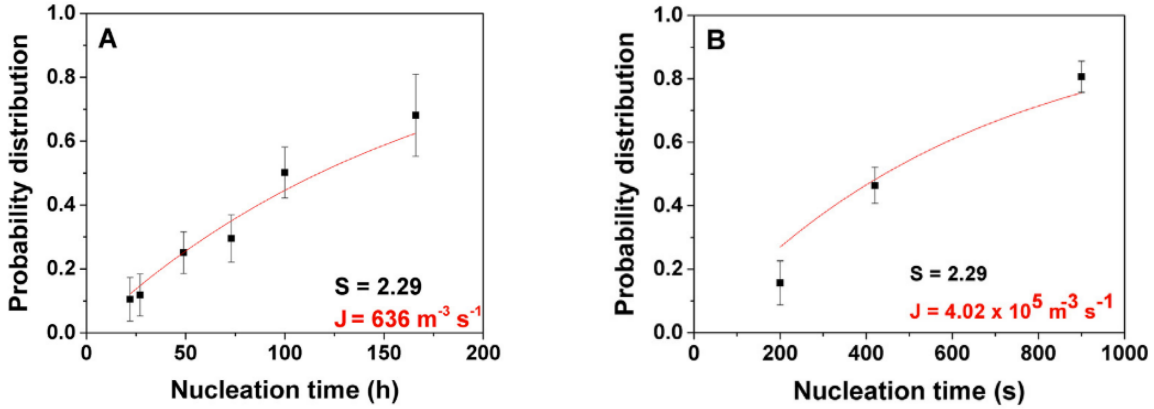

(a) (b)

Figure 8 Nucleation rate for stagnant and flowing droplets for crystallization of PABA in **(a)** stagnant conditions (S=2.29) and in **(b)** flowing conditions (S=2.29)[127]. Reprinted with permission from Chem. Eng. Res. Des. 2018, 136, 48–56. Copyright (2018) Elsevier.

Time-varying supersaturation droplet technique

Goh *et al.* developed a model in the form of a master equation to determine nucleation kinetics in droplet-based system under conditions of time-varying supersaturation (*e.g.* in evaporation-based systems where heat is supplied)[66]. $P_0(t)$ is defined

as the probability that a droplet contains 0 crystals (with $P_0(0) = 1$) at time t, and $P_n(t)$ is the probability that a droplet contains n crystals (with $P_n(0) = 1$) at time t. Goh *et al.*'s master equation is shown in eq. 67 and eq. 68 [66].

$$\frac{dP_0(t)}{dt} = -J(t) \cdot P_0(t) \quad (67)$$

$$\frac{dP_n(t)}{dt} = -J(t) \cdot \left(P_{n-1}(t) - P_n(t)\right) \quad \text{for } n = 1, 2, \ldots \quad (68)$$

Goh *et al.* derive eq. 69 to determine the nucleation kinetics from experimental data, by least-squares estimation[66].

$$\min_{A,B} \sum_{i=1}^{n_{\text{exp}}} \sum_{k} \left[\ln\left(P_{0,i}\left(t_k\right) + \int_0^{t_k} J\left(S_i(S)\right) \cdot V_i(S) dS\right)\right]^2 \quad (69)$$

Advantages: (i) The model proposed by Goh *et al.* can be applied for both homogeneous as heterogeneous nucleation in a wide range of experimental conditions. **(ii)** Has the same advantages as the isothermal droplet technique. **(iii)** The assumption that growth of crystals does not deplete the supersaturation is not required[66]. **Disadvantages: (i)** Bhamidi *et al.* give a complete overview of the assumptions the Goh *et al.* model makes[64]. The Goh model relies (similarly to the MNM description of nucleation) on the Markovian approximations: *e.g.* the system can only jump from *m* to *m+1*, thus assuming jumps from *m* to *m+2* are negligible[64]. Because of the time-varying supersaturation additional assumptions are required: the nucleation rate *J* changes between two successive time steps but not in between, and the time steps are long enough for the system to reach equilibrium[64]. **(ii)** It is assumed that all nucleation steps take place independently from the number of crystals already present[64]. **(iii)** The same disadvantages as the conventional droplet technique. **(iv)** The method is computationally more difficult than the isothermal method.

Table 6 Overview of papers describing using the droplet method (possibly in combination with the double-pulse technique) to determine nucleation rates with a short description of the system. For all experiments summarized in the table the onset of nucleation is detected using a microscope.

Authors and year	Crystallization solute	System
Galkin and Vekilov (1999, 2000, 2001)[34,105,129]	Lysozyme (50mg/mL-78mg/mL) in water with acetate buffer (pH=4.5), c_{NaCl}=2.5-4%	Double-pulse, stagnant droplets (400 wells, 0.1-2.5μL, usually 0.7μL),
Knezic *et al.* (2004)[130]	Lysozyme (4wt%) in water with 0.1M acetate buffer (pH=4), c_{NaCl}=1%	Levitated droplet method (225fL),
Chen *et al.* (2005)[128]	Thaumatin and precipitant (2M)	Droplet method (50 droplets)
Shim *et al.* (2007)[131]	Xylanase (15.3mg/mL) dialyzed against sodium tartrate tetrahydrate 0.4M, c_{NaCl}=5M	Double-pulse technique (with seeding), stagnant droplets (Phase Chip, 100 wells, 1nL)
Dombrowski *et al.* (2007)[132]	Lactose in water (35-53g/100g)	Flowing droplet technique (100-300μm)
Laval *et al.* (2007)[101]	Potassium nitrate in water (83.6g/100g)	Flowing droplet method (100nL, 4mm s^{-1})
Laval *et al.* (2009)[118]	Potassium nitrate in water (30-70g/100g)	Stagnant droplet method (300 droplets, 100nL)
Selimović *et al.* (2009)[133]	Lysozyme (17.5g/mL) in water with acetate buffer (pH=4.5), c_{NaCl} = 0.5M	Double-pulse technique, stagnant droplets (Phase Chip[131], 300 wells, 1.4nL)
Goh *et al.* (2010)[66]	Lysozyme (18mg/mL) in water, c_{NaCl} = 0.36M & paracetamol in water	Droplet method (evaporation, open well, min. 100μL)[134]
Teychené and biscans (2011, 2012)[116,123]	Eflucimibe in octanol	Stagnant (1500-2000 droplets, 10-100nL) or flowing droplet method (10-100nL)
Ildefonso *et al.* (2011, 2012 (MZW), 2013)[72,107,135]	Lysozyme (40-55g/mL) in water with acetate buffer (pH=4.5), c_{NaCl}=0.7M	Double-pulse technique, stagnant droplet method (200 droplets, 250nL)[72,107,135]
Wantha *et al.* (2012)[136]	γ-DL-methione in water	Double-pulse technique, stagnant droplet method (0.2μL, 25 wells)
Chen *et al.* (2012)[46]	Paracetamol in water, glycine in water	Stagnant droplet technique (paracetamol: 5.07μL, glycine: 4.50μL)

Akella *et al.* (2014)[125]	Lysozyme in 12.5%w/v polyethylene-glycol (pH=4.8), c_{NaCl}=5%w/v	Flowing droplet method, (1000-4000 drops, <1nL, 300μL h^{-1})
Rossi *et al.* (2015)[45]	Adipic acid in water	Double-pulse technique, stagnant and flowing droplets (1.5μL)
Lu *et al.* (2015)[137]	Lactose in water, aspirin in ethanol	Stagnant droplet-based (air-segmented) technique (65 droplets, 711μm)
Zhang *et al.* (2015)[138]	Rasburicase (biological macromolecule) in viscous medium (with PEG as precipitant agent) in oil	Stagnant droplet method (65 and 100nL,100-200 droplets)
Selzer *et al.* (2018)[139]	Potassium nitrate in water and EGDS in water	Flowing droplet method (400 droplets, 20-90nL)
Nappo *et al.* (2018)[127]	para-Aminobenzoic acid (PABA) in water	Double-pulse technique, flowing (4μL, 2.12mm s^{-1}) and stagnant droplets (400, 4μL)
Ferreira *et al.* (2018)[140]	Lysozyme (17.5g/mL) in water with acetate buffer (pH=4.7), c_{NaCl}=3%(w/v)	Droplet method (250 droplets, 0.9-18μL)
Dos Santos *et al.* (2019)[122]	Adipic acid in water	Stagnant or flowing droplet method (1000 droplets, 167nL)

Isothermal microvial technique

The droplet method offers a unique environment for nucleation rate determination, but is also limited in its experimental operating range. Particularly the effects of agitation on the nucleation rate are impossible to quantify in droplets. Jiang and Ter Horst have proposed a method for nucleation rate determination in (stirred) microvial crystallizers (1-10mL), by measuring the variance in the induction times[2,141]. They proposed to measure the variance in the induction times in small stirred microvials[2]. The experimental probability $P_{exp}(t)$ that at least 1 nucleus after time t is detected, can be found by taking the ratio of experiments containing at least 1 nucleus after time t and the total amount of experiments preformed, as is shown in eq. 70. $M_{\geq 1}(t)$ is the number of experiments for which a crystal has been detected before time t, and M_{tot} the total number of experiments.

$$P_{exp}(t) = \frac{M_{\geq 1}(t)}{M_{tot}} \qquad (70)$$

The MNM for isothermal measurements has a theoretical formula for the probability of detecting at least 1 nucleus before a time t, which is shown in eq. 12. Fitting eq. 12 to the experimental probability gives a value for the nucleation rate (JV) and the growth time (t_g). The A and B parameters can then be found by determining the nucleation rate for different supersaturation ratios. This is illustrated in Figure 9.

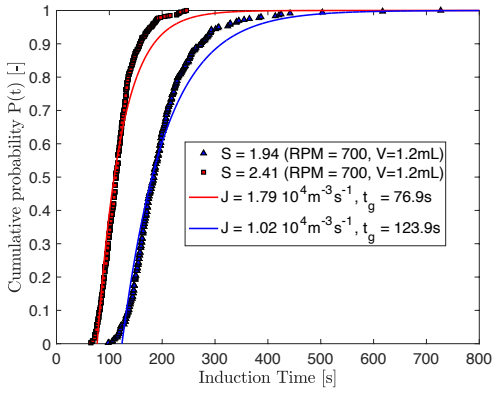

Figure 9 The microvial technique for paracetamol in water performed in a Crystal16 device (RPM=700, V=1.2mL, unfiltered). The red squares and blue triangles are the experimental data points (eq. 78). For S=1.94 and 2.41, respectively, 361 and 665 measurements were performed. MNM eq. 79 is fitted to the experimental cumulative probability (A=1.17·10^{4}m^{-3}s^{-1}, B=0.351).

Advantages: (i) This method offers a wider experimental range compared to the droplet technique (*e.g.* stirring), which makes it easier to mimic industrial crystallizers. **(ii)** It is easy to gather large amounts of data as these experiments are often performed in well-controlled[116] multivial systems. The group of Ter Horst used the Crystal16 device (Technobis Crystallization Systems B.V, graphically illustrated in Figure 10), which consists of 16 temperature-controlled 1.2mL microvials that can be stirred using magnetic stirrers or overhead stirrers and the Crystalline device (Technobis, Crystallization System B.V.) with 8 3mL vials[2,70,71,102]. The group of Rasmuson has developed their own multicell devices like the 'multicell nucleation block' which is designed for 15 parallel induction time measurements in cells of

6mL[142] and a multivial system with 30 20mL vials[51]. Similarly, the group of Sefcik has a custom induction platform with 8mL vials[143]. These multivial systems are ideal for performing simultaneous parallel stochastic nucleation measurements. Some authors have used lithography to develop microbatch platforms. For example Juárez-Martínez *et al.* have developed a micro-array (100 batches, 500μL) for protein crystallization[144]. **(iii)** One additional advantage is that it is easier to compare crystallizations of different compounds, as the setup is kept constant as opposed to the droplet technique, for which droplet characteristics may different between different compounds. Table S2 gives an overview of nucleation rate constants determined in the Crystal16. **Disadvantages: (i)** Experiments require more time. In the droplet technique, on the other hand, more than 100 droplets (batches) can be studied simultaneously (*e.g.* Laval's microfluidic setup allows storage of 300 monodisperse droplets of 100nL[118], Teychené and Bicans setup allows storage of up to 2000 droplets of 11nL[116]). **(ii)** The MNM equations are used, which means the conditions of the MNM theory must be met (Subsection: Isothermal and Polythermal experiments). In particular the condition that all nuclei must be formed independently from each other, is never fulfilled. **(iii)** Detection is more complicated because of the larger volume compared to the droplet technique. **(iv)** Increased probability of secondary nucleation compared to the droplet technique. **(v)** The microvial wall provides an interface for crystals to nucleate on ('crowning'[145]). If crystals stay on the microvial wall this also affects the detection of crystals. **(vi)** It is assumed that the growth kinetics are the same for experiments with the same conditions or sufficiently high to be negligible[146]. **(vii)** The model does not take into account the relaxation time for nucleation[146].

Polythermal microvial technique

A polythermal microvial technique was proposed by Kulkarni *et al.*[147]. A cumulative probability of nucleation is determined experimentally by taking the ratio of experiments where at least 1 nucleus has nucleated within a temperature range ΔT and the total number of experiments. Eq. 14 is then fitted to the experimental cumulative probability curve, shown in eq. 71.

$$P_{\text{exp}} = \frac{M_{\geq 1}(\Delta T)}{M_{\text{tot}}} \tag{71}$$

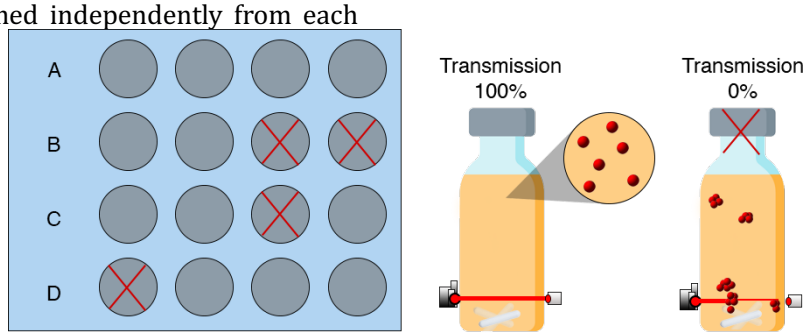

Figure 10 Graphical representation of the Crystal16 microvial setup, with the cross indicating the vials in which crystallization has occurred.

Advantages: (i) The same advantages as the isothermal microvial technique. **(ii)** Less labor intensive and easier to analyze compared to the induction time method[147]. **Disadvantages: (i)** The same disadvantages as the isothermal microvial technique. Also, the nucleation rate is assumed to be constant during one time step, but changes during successive time steps (because the supersaturation changes)[64]. **(ii)** The MZW is strongly dependent on the cooling rate: high cooling rates can result in very large MZWs. This "overshooting effect" can result in different *A, B* values that do not reflect the true nucleation rate. This makes the technique less accurate than the isothermal technique. **(iii)** The temperature control is more difficult compared to the isothermal microvial technique[147].

Kulkarni *et al.* has performed the isothermal and polythermal microvial technique for crystallization of INA in ethanol in the Crystal16 (V=1mL, RPM=700)[147]. The obtained results (see Table S2) show large differences for low cooling rates and only little differences for higher cooling rates (*A* for the isothermal technique $6.6 \cdot 10^3 m^{-3}s^{-1}$, for the polythermal technique $0.42\text{-}5.8 \cdot 10^3 m^{-3}s^{-1}$ for cooling rates from 0.1 to 1°C/h; *B* for the isothermal technique 0.32, for the polythermal technique 0.02-0.89 for cooling rates from 0.1 to 1°C/h)[147]. The isothermal and polythermal technique are closely related, but even for the same setup (Crystal16, same volume, same stirring) and the same solution significantly different values are obtained.

Other microvial techniques

Darcy and Wiencik studied lysozyme (in water with acetate buffer (pH=4.6), c_{NaCl} = 3-5%) in three 1mL sample cells using microcalorimetry[61]. The heat released during the crystallization process (enthalpy) was recorded and used to estimate crystal growth rates[61]. Dixit *et al.* calculated an extreme upper bound for the nucleation rate by neglecting crystal growth and assuming all the heat was released during the nucleation process if the critical radius of lyzosyme is 4 molecules[108].

PART III: CRITICAL DISCUSSION

Experimental nucleation rate determination is crucial for two reasons. Knowledge of the nucleation rate helps in the design and control of industrial crystallizers; and in uncovering the mechanism of nucleation. The experimental large volume batch methods, described in **Part I** of this review, offer an easy way to characterize the kinetic and thermodynamic behavior of the crystallizing system. The Nývlt and similar methods usually fail in providing mechanistic insights into nucleation. This has changed somewhat with the development of the KBHR model, which makes it possible to distinguish between PN and IN nucleation. Nevertheless, large volume batch nucleation rate determination does not capture the physical reality of primary nucleation. The development of microfluidic platforms has resulted in a more systematic way of determining the experimental nucleation rate. Microfluidic methods rely on the stochastic nature of nucleation, which require a lot of experiments under identical conditions in small volume crystallizers. One criticism is that these platforms often fail to predict the behavior of the system in large scale crystallization processes. It seems that these models provide no alternative to the traditional large volume batch models for process control and characterization, but are instead becoming a distinct step in the design of new crystallization processes. They are ideal for high-throughput screening and they offer fundamental insight into the nucleation process[11]. In particular the extreme control over the process conditions and the possibility to decouple nucleation and growth is useful.

How should we interpret the results from the models for nucleation rate determination discussed in this review and which model must be selected for which application? This discussion highlights two important topics that are relevant in the selection of methods: scale-up, and secondary nucleation. In any case, a researcher aiming to determine the nucleation kinetics must always remain thoughtful of the limitations of the model and setup that is employed.

Scale-up?

Can nucleation rates determined in small volume (microvial or microfluidic) crystallizers be used to determine nucleation rates in large volume crystallizers? The nucleation rate is defined as intensive property (new nuclei per volume per time). MZWs and induction times, on the other hand, cannot be considered properties that are independent of volume. Kubota explains the influence of volume on the MZW by looking at the number of nuclei being produced per time (JV)[17]. Larger volumes result in increased nucleation probabilities and thus a higher probability of nuclei appearing sooner. According to Kubota, the effect of volume disappears if turbidity is used to detect the onset of nucleation (N_{det}/V)[17]. We do not agree with this last statement as the rate of secondary nucleation due to stirring strongly affects the final results and it is unsure how this scales with volume.

Induction times for L-glutamic acid measured with FBRM and ATR-FTIR in a 0.5L and 2L crystallizer matched well[148,149]. Kadam *et al.* studied the MZW for paracetamol in water crystallization at 1mL (Crystal16, 700RPM, turbidity detection, CR=0.5°C/min) and 1L (stirred at 700RPM, camera detection, CR=0.5°C/min) scales[70]. In the 1mL crystallizer a MZW distribution is obtained, in the 1L crystallizer only a spread of 0.5°C around an average value was observed[70]. The lowest MZW value obtained in the 1mL is approximately the value obtained in the 1L crystallizer. This could potentially be used as a rule for scale-up. Kadam *et al.* explain this observation via the SNM: in both crystallizers a single nucleus nucleates, which then undergoes secondary nucleation[70]. In the large volume crystallizer the probability of nucleation of this first nuclei is higher than in the small volume crystallizer. In a later paper, Kadam *et al.* studied the MZW of paracetamol in water and isonicotinamide (INA) in ethanol for varying volumes from 1mL to 1L (cooling rate of 0.5°C/min, 350RPM)[71]. They found that the MZW is not reproducible, but a distribution, with increasing variability for smaller volumes, is developed below a transition temperature. Above this transition temperature it becomes a deterministic property[71]. The MZW measurements from Kadam *et al.* are shown in Figure 11[71].

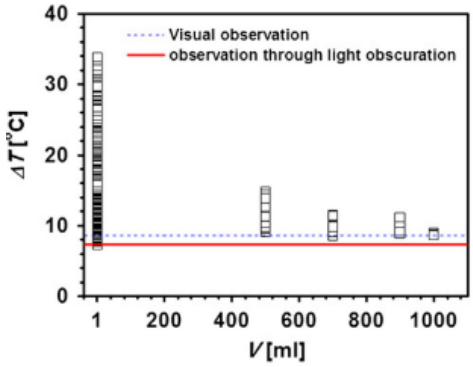

Figure 11 MZW measurements for different volumes for an aqueous solution of paracetamol (CR=0.5°C/min)[71]. Reprinted with permission from Chem. Eng. Sci. 2012, 72, 10–19. Copyright (2012) Elsevier.

Nordström *et al.* also studied the effect of solution volume on the MZW of salicylamide in methanol (15, 150 and 500mL) using a camcorder[150]. They found that the onset of nucleation was unaffected by solution volume[150], which contradicts the experimental observations by Kadam *et al.* and the SNM[150]. If the PNM is correct multiple nuclei grow at the same time to a detectable size, which increases the probability of the MZW being perceived as a deterministic volume independent property.

Steendam *et al.* studied the effect of volume on the nucleation rate of paracetamol in 2-propanol by comparing the results for volumes of 10mL, 85mL, 340mL and 680mL[68]. The isothermal microvial technique is used, with an FBRM to detect the onset of nucleation in volumes larger than 10mL and a camera for the 10mL crystallizer. The nucleation rate for the smallest volume (10mL) was significantly higher than the nucleation rates for the larger volumes (85-680mL), which were more similar to each other (Table S3). The thermodynamic nucleation parameter only changed slightly, whilst the kinetic nucleation parameter changed significantly from the smaller to the larger volumes. It must be noted, however, that only the 10mL vial was stirred using a magnetic stirrer, compared to an overhead stirrer for the other crystallizers. Steendam *et al.*'s results may indicate that the nucleation rate does not depend strongly on the solution volume, but rather on the shear rate caused by stirring[68]. Laval *et al.* studied the effect of droplets volume on *JV* for volumes between 0.1 and 0.2μL in the flowing droplets technique[101]. In this small range of volumes, the *JV* values were found to be proportional to the volume suggesting that nucleation rates are independent of volume.

Cedeno *et al.* observed a major discrepancy in the nucleation rates from isothermal microvial experiments (in 1mL), compared to the nucleation rate by direct particle-counting (3D ORM) in a larger crystallizer (100mL) (for PABA and LGA, see Table S2, Table S3)[53]. Cedeno *et al.* rule out that this discrepancy is caused by breakage and attrition and conclude: "these results provide strong evidence that nucleation rates obtained from the stochastic model may not be used as a reference for scale-up and design of industrial crystallizers"[53].

Candoni *et al.* note that in extremely small volumes (in the range of 100nL) there is a kinetic limitation to induction time studies: the induction times become extremely long[67]. For even smaller volumes (pL-fL) apart from this kinetic limitation also a thermodynamic limitation exists (the confinement effect)[67,151]. Due to confinement the solution properties change significantly during the formation of the critical cluster, which makes the CNT invalid for such small volumes[67] and allows the existence of extremely high supersaturations[151]. Grossier *et al.* have used the confinement as an advantage to initiate a heterogeneous nucleation event by touching the oversaturated solution with a sharp tip[151].

We conclude that experimentally determined nucleation rates in microfluidic droplet crystallizers are probably the best indication of the inherent metastability of the system and may possibly be used to get an idea of the lower bound nucleation rate values in larger scale volumes. In microvial and large volume crystallization it is clear that the process conditions (turbulence, energy input, impurities, surface material[62]) play a pivotal role in the measured nucleation kinetics. In particular, the role of secondary nucleation may affect the behavior of the system. Based on the existing literature it is difficult to formulate a scaling rule. Therefore, it is advised to use the microvial methods cautiously as high-throughput screening methods for nucleation rate determination. The discussed results highlight the importance of an in-depth understanding of the secondary effects that play a role, to understand and interpret results from nucleation rate experiments.

Stirring?

Stirring increases the nucleation rate, both in small (e.g. 10mL[152]) and large volume crystallizer[67]. Secondary nucleation is strongly affected by agitation. In contrast, it remains unknown to what extent stirring affects primary nucleation[53,152]. Recent research suggests that shear affects the nucleation rate. As mentioned in Subsection "Scale-up?" Steendam *et al.* hypothesizes that the differences in shear rate in different volume crystallizers (10-680mL) affect the nucleation rate[68]. Liu and Rasmuson have used

a Taylor-Couette cell to show that nucleation rates increase for increasing shear rates. Forsyth *et al.* found similarly that shearing a supersaturated aqueous glycine solution (in a Taylor-Couette flow cell and a capillary crystallizer) resulted in lower induction times[153,154]. These results may be explained by the existence of agitation-enhanced mesoscale clusters[51,153,154]. Similar observations have been made in microfluidic crystallizers. Nappo *et al.* finds higher nucleation rates for flowing droplets compared to stagnant droplets (see Figure 8)[127]. A similar observation was made by Rossi *et al.*[45].

An increase in the agitation does not just imply a similar increase in the nucleation rate in batch crystallizers. Liu and Rasmuson have shown that the induction time of butyl paraben in ethanol decreased with increased stirring (magnetic stirrer) in small vials (20mL), but a further increase resulted in longer induction times (as shown in Figure 12)[51]. Similar observations had already been reported by Mullin and Raven[51,155].

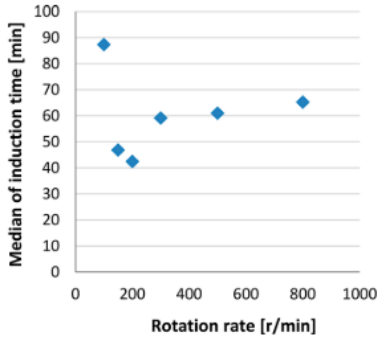

Figure 12 The median induction time in small vials for varying stirring rates for a fixed supersaturation[51]. Reprinted with permission from Cryst. Growth Des. 2013, 13, 10, 4385–4394. Copyright (2013) American Chemical Society.

Secondary nucleation?

Secondary nucleation causes an increase in the total nucleation rate, but how this exactly happens is still not clear[156,157]. It is impossible to know with certainty whether crystals originate from primary or secondary nucleation (even when using seeds with different polymorphs or chirality[157,158]). In Figure 13 a graphical representation of some possible secondary nucleation mechanisms is shown. A more in depth discussion of the mechanisms of secondary nucleation can be found in the paper of Agrawal *et al.*[159] and in the Handbook of Industrial Crystallization[160,161].

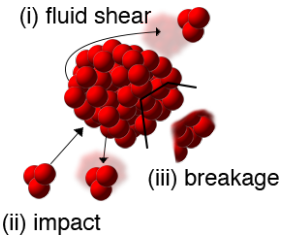

Figure 13 Graphical representation of secondary nucleation from parental crystal mechanisms: (i) fluid shear causing the removal of a solute layer, (ii) impact (crystal-crystal, crystal-impeller) causing attrition or the removal of a solute layer, (iii) breakage (or fragmentation) due to mechanical impact

The probability of a crystal hitting the impeller is large in small stirred microvials, compared to the probability in large batch crystallizers[68]. In microvials sometimes a single crystal causes a sudden increase in the number of crystals[156]. According to the SNM, nucleation occurs via the formation of a single crystal, which then grows and undergoes secondary nucleation (via crystal-impeller attrition)[70], as is shown in Figure 14. Attrition in microvials was also studied by Bosetti *et al.*[162]. They conclude that understanding the fluid dynamics is crucial in obtaining insights into secondary nucleation[162]. The importance of mixing and its effect on the induction time for antisolvent crystallization was also highlighted by Ramakers *et al.*[143]. Ramakers *et al.*'s results for antisolvent glycine crystallization may be an indication that secondary nucleation and crystal growth become the rate limiting step at high supersaturations[143]. Briuglia *et al.* have shown that for seeding a single crystal in a stirred microvial, secondary nucleation might be negligible below a supersaturation threshold[163]. Cedeno *et al.* extrapolated their results for different agitation rates to zero agitation, to remove the effect of secondary nucleation (assuming the primary nucleation rate is unaffected by stirring)[53]. More research is required to completely characterize the role of secondary nucleation in these systems and to what extent the nucleation rate measurements are actually measuring primary nucleation.

In large volume stirred batch crystallizers it is even more difficult to quantify the effect of secondary nucleation. Tyrrell *et al.* have shown that the fluid dynamics of a moving impeller might protect crystals from attrition in a large volume crystallizer[164]. Protection from the impeller alone is, however, not enough to prevent secondary nuclei: experiments have shown that fluid flow (shear) is sufficient to generate secondary nuclei[165], although it has also been reported that this shear nucleation might be less effective[166].

In the stagnant droplet and double-pulse technique solutions are not stirred, so nucleation

rates measured using these methods are expected to be the closest to the primary nucleation rates.

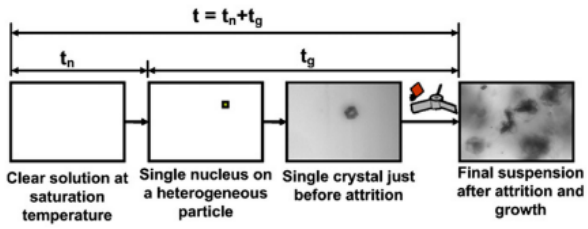

Figure 14 Explanation of the SNM in an isothermal measurement, with t_n the nucleation time and t_g the growth time. From Kadam *et al.*[71]. Reprinted with permission from Chem. Eng. Sci. 2012, 72, 10–19. Copyright (2012) Elsevier.

Future work

A lot of advances have been made in the field of experimental nucleation rate determination, since the development of microfluidic and microvial methods. Nevertheless, there is still work to be done. Firstly, it is important that authors clearly list the limitations of their experiments and their mathematical models. In particular, all the possible causes for deviations from primary nucleation must be reported. This would allow valuable comparisons of nucleation rates between different papers. Secondly, more experimental work is required to obtain a fundamental mechanistic understanding of nucleation. New crystal detection techniques may open the door to insights on a molecular scale[11]. Other studies could assess the importance of secondary nucleation and the influence of hydrodynamics on the nucleation rate. There has been some physical evidence for the existence of mesoscale clusters[167–172], but more work is required to establish their existence and understand their behavior in organic crystallization. Thirdly, there is a need for a more advanced theory of nucleation, that includes molecular interactions and accurate quantitative descriptions of homogeneous, heterogeneous and secondary nucleation. Lastly, efforts to simplify complex theoretical models into easy-to-use ones will also be valuable. Experimental nucleation rate determination will continue to be a balance between difficult-to-use advanced models and fast easy models that rely on a number of assumptions.

CONCLUSION

A critical overview of experimental nucleation rate determination methods was presented, with a strong focus on polythermal and isothermal data analysis methods for both large volume batch crystallizers (**Part I**) and small volume microfluidic and microvial crystallizers (**Part II**). The review also summarizes the published nucleation rate values (**SI**) and reflects on nucleation rate experiments in the discussion section (**Part III**). This review highlights the importance of, firstly, a carefully thought-out method selection, as it can influence the result dramatically and, secondly, an understanding of the assumptions on which the models are based. This review can serve as a first step for researchers aiming to experimentally characterize the nucleation process. The tables in the SI can form a starting point in the design of the experiment.

Large volume batch crystallizer methods remain an integral part of the design and control of industrial crystallizers. The development of microfluidic and microvial methods has opened new pathways for a mechanistic understanding of nucleation. These methods rely on the stochastic nature of nucleation to determine the nucleation rate. In particular high-throughput testing is attractive for obtaining insights into the nucleation process, but their failure to mimic the conditions of industrial crystallizers makes microfluidic crystallizers difficult to use for industrial process design. As a general rule, qualitative comparisons can be made between different models and setups, but quantitative comparisons require established protocols for experimental nucleation rate determination.

ASSOCIATED CONTENT

Supporting Information

The Supporting Information is available free of charge on the ACS Publications website.

Table S1 with the different definitions of the nucleation rate equation from the CNT; Table S2 with published nucleation rate (A, B)-parameters from Crystal16 measurements for different compounds, solvents and methods; Table S3 with published nucleation rate (A, B)-parameters from literature for a variety of compounds, solvents, methods, setups and detection techniques; Table S4 with nucleation rate experiments from literature for a variety of compounds, solvents, methods and detection techniques (PDF).

AUTHOR INFORMATION

Corresponding Author

* E-mail: simon.kuhn@kuleuven.be

Author Contributions

All authors have given approval to the final version of the manuscript.

ACKNOWLEDGMENT

C.D. thankfully acknowledges FWO Flanders for a Fundamental PhD fellowship (11H4421N). S.K. acknowledges support from the Research Foundation Flanders (FWO).

ABBREVIATIONS

CNT	Classical Nucleation Theory

CSD	Crystal size distribution
eBVI	External bulk video imaging
eq.	Equation
FBRM	Focused beam reflectance measurement
IN	Instantaneous nucleation
INA	Isonicotinamide
IVM	Inline video microscopy
MNM	Mononuclear nucleation mechanism
MSMPR	Mixed suspension mixed product removal crystallizer
MZW	Metastable zone width
ORM	Optical reflectance measurement
PABA	para-Aminobenzoic acid
PBE	Population balance equation
PN	Progressive nucleation
PNM	Polynuclear nucleation mechanism
PVM	Particle vision measurements
SI	Supplementary Information
SNM	Single Nucleus mechanism
US	Ultrasound

NOMENCLATURE

Greek script

α_{det}	ratio of the crystalline volume and the solution volume	-
α	fraction of crystallized volume	-
γ	interfacial tension (between the crystalline surface and the solution)	J/m²
υ	molecular volume of the crystal	m³
ρ	density of a crystal	kg/m³
Δρ	mass based supersaturation	kg/m³
$\Delta\rho_{\mathrm{max}}$	mass based supersaturation at the MZW	kg/m³
$\Delta\mu$	the chemical potential difference of the solute	J/mol
$\kappa(t)$	the time-dependent rate of nucleation	s⁻¹
ε	hydrate conversion factor	-
σ	specific energy of a crystal compared to the solution	Pa
ϕ	slope in Sangwal's self-consistent Nývlt-like equation	-
Γ	parameter in Kubota's stochastic model	-
φ_{HE}	heterogeneity factor	-
φ_{M}	volumetric hold up of crystals	-
ζ	molecular latent heat of crystallization	J
μ_j	j'th moment	m^j
τ	mean residence time	s

Latin script

A	pre-exponential kinetic nucleation parameter or parameter in the KBHR model	m⁻³s⁻¹
A_c	crystal surface	m²
A_{HO}	pre-exponential kinetic nucleation parameter for homogeneous nucleation	m⁻³s⁻¹
A_{HE}	pre-exponential kinetic nucleation parameter for heterogeneous nucleation	m⁻³s⁻¹
a	dimensionless molecular latent heat of crystallization	-
a_i	activity	-
$a_{i,\mathrm{sat}}$	activity of a saturated solution	
B	thermodynamic nucleation parameter	-
b	dimensionless thermodynamic nucleation parameter	-
c	concentration	mol/m³ or kg/kg
c_c	molar density of the crystal	mol/m³
c_{eq}	equilibrium concentration (as a function of temperature)	mol/m³
c_N	solution concentration expressed as anhydrous mass per unit mass of solvent at a certain temperature	kg/kg
c_1	concentration at T_1	mol/m³
c_0	concentration of active nucleation sites or concentration at T_1	m⁻³ or mol/m³
$c_{\mathrm{max,eq}}$	equilibrium concentration at T_{max}	mol/m³ or kg/kg
$c_{0,\mathrm{HO}}$	concentration of active nucleation sites for homogeneous nucleation	m⁻³
$c_{0,\mathrm{HE}}$	concentration of active nucleation sites for heterogeneous nucleation	m⁻³
Δc	concentration difference ($\Delta c = c - c_{\mathrm{eq}}$)	mol/m³ or kg/kg

$\Delta c_{\max}$	the concentration difference between the MZW concentration and the equilibrium concentration	mol/m³ or kg/kg
D_{AB}	diffusion coefficient	m²/s
d_g	growth dimensionality	-
d_m	molecule diameter	m
E	efficiency factor for surface nucleation in the Kim and Mersmann model	-
F_1	parameter in Sangwal's second model	-
f_c	constant number of entities	1/m³
f_M	reduction factor	-
f_n	size distribution	1/m³
f^*	attachment frequency	s^{-1}
g	growth rate order	-
G	growth rate	m/s
ΔG	free energy change required for cluster formation	J
ΔG_v	volume contribution of the free energy change required for cluster formation	J
ΔG_{crit}	critical free energy barrier for nucleation	J
ΔH_s	the heat of dissolution	J/mol
J	nucleation rate	m^{-3}s^{-1}
J_{HO}	homogeneous nucleation rate	m^{-3}s^{-1}
J_{HE}	heterogeneous nucleation rate	m^{-3}s^{-1}
J_{sur}	surface nucleation rate	m^{-3}s^{-1}
J_{att}	attrition nucleation rate	m^{-3}s^{-1}
J_m	nucleation rate in mass basis	g/h
K	parameter in Nagy *et al.* model	-
k	nucleation rate constant (e.g. in $J = k\Delta c_{\max}^n$) and in Sangwal model	1/m³s or m^{-3}s$^{-1}\cdot\Delta c_{\max}^{-n}$
k_{HO}	homogeneous nucleation rate in a Pound and La Mer equation	s^{-1}
k_{HE}	homogeneous nucleation rate in a Pound and La Mer equation	s^{-1}
k_v	the volume shape factor	- or m^{3-d}
k_m	nucleation rate in mass basis (*e.g.* in $J_m = k_m\Delta c_{\max}^n$)	1/s with $\Delta c_{\max}$ kg/kg
k_{b}	Boltzmann constant	$1.38\cdot10^{23}$ J/K
k_g	the growth rate constant	m s$^{-1}\cdot\Delta c^{-g}$ or m$^{1/m}$s^{-1}
k′	nucleation rate constant	K^{-n} m^{-3}s^{-1}
L	characteristic size of the crystals	m
M	parameter in the Nývlt model or the mass of all crystals	kg/kg K or kg
M_P	parameter in Preckshot *et al.* model	-
M_W	molecular volume	m³/mol
M_{tot}	total number of experiments	-
$M_{\geq1}(t)$	number of experiments for which a crystal has been detected before time t	-
$M_{\geq1}(\Delta T)$	number of experiments for which a crystal has been detected within a temperature difference	-
m	apparent nucleation rate order in Nagy *et al.* model	-
m(t)	mass of a crystal nucleated time t ago	kg
m_{avg}	arithmetic average number of active foreign nucleation sites per droplet in the Pound and La Mer equation	-
m_g	growth exponent (positive number)	-
N	number of crystals, or the total number of droplets, or number of crystals per volume (in Mersmann models)	- or m^{-3}
N_0	number of droplets with no nuclei	-
N_t	total number of droplets	-
N_c	number of droplets with crystals	-
N_A	Avogadro constant	mol^{-1}
N_{det}	number of crystals at detection	-
N_m	total number of crystals nucleated in time t_{end}	-
n	nucleation rate order;	-
n_p	molecular protein concentration	g/L
n_g	growth exponent (positive number)	-
P	probability of nucleation	-
P_0	the probability that nucleation has not yet occurred	-
P_{exp}	experimentally determined probability	-

$P_{0,exp}$	experimentally determined probability that nucleation has not occurred	-
P_m	probability of forming m nuclei (N)	-
$P_{\geq 1}$	probability of forming at least 1 nuclei (N)	-
$P(t)$	probability of at least 1 nuclei (N) being formed before time t	-
Q_k	flow in or out the crystallizer	m^3/s
q	cooling rate	K/s
R_n	ratio of molecular weights of the hydrate and anhydrous salt	-
R_G	ideal gas constant	$J{\cdot}mol^{-1}K^{-1}$
r	radius of a crystal or nucleus	m
r_{crit}	radius of a critical nucleus	m
r_{det}	radius of a detectable crystal at the maximum supersaturation	m
S	supersaturation ($S = c/c_{eq}$)	-
S^*	alternative supersaturation definition ($S^* = (c - c_{eq})/c_{eq}$)	-
S_{MZW}	supersaturation at the MZW	-
S_{max}	supersaturation at which crystals are detected	-
$S_{max,hom}$	supersaturation at which crystals are detected, for homogeneous nucleation;	-
$S_{max,surf}$	supersaturation at which crystals are detected, for surface nucleation	-
T	temperature	K
T_c	crystallization temperature	K
T_{det}	temperature at which crystals are detected	K
T_{eq}	equilibrium temperature	K
ΔT_{max}	MZW ($\Delta T_{max} = T_{det} - T_{eq}$)	K
ΔT	temperature difference	K
t	time	s
t_{det}	time at which crystals are detected	s
t_{ind}	induction time	s
t_{PNM}	induction time assuming the PNM is correct	s
t_{MNM}	induction time assuming the MNM is correct	s
t_{sat}	latest time at which the solution was saturated	s
t_r	relaxation time	s
t_n	nucleation time	s
t_g	growth time	s
u	the undercooling	K
u_c	critical undercooling in the KBHR model	-
V	volume	m^3
V_m	the volume of a detectable nuclei	m^3
V_c	crystalline volume	m^3
Z	Zeldovich factor	-

REFERENCES

(1) Erdemir, D.; Lee, A. Y.; Myerson, A. S. Nucleation of Crystals from Solution: Classical and Two-Step Models. *Acc. Chem. Res.* **2009**, *42* (5), 621–629. https://doi.org/10.1021/ar800217x.

(2) Jiang, S.; Ter Horst, J. H. Crystal Nucleation Rates from Probability Distributions of Induction Times. *Cryst. Growth Des.* **2011**, *11* (1), 256–261. https://doi.org/10.1021/cg101213q.

(3) Lührmann, M. C.; Termühlen, M.; Timmermann, J.; Schembecker, G.; Wohlgemuth, K. Induced Nucleation by Gassing and Its Monitoring for the Design and Operation of an MSMPR Cascade. *Chem. Eng. Sci.* **2018**, *192*, 840–849. https://doi.org/10.1016/j.ces.2018.08.007.

(4) Nývlt, J.; Söhnel, O.; Matachová, M.; Broul, M. *The Kinetics of Industrial Crystallization*; Elsesevier Science Publishers, 1985.

(5) Tavare, N. S. Batch Crystallizers: A Review. *Chem. Eng. Commun.* **1987**, *61* (1–6), 259–318. https://doi.org/10.1080/00986448708912042.

(6) Tavare, N. S. *Industrial Crystallization - Chapter 3: Crystallization Kinetics*; Springer International Publishing, 1995. https://doi.org/https://doi.org/10.1007/978-1-4899-0233-7_3.

(7) Mullin, J. W. Book Review: Measurement of Crystal Growth and Nucleation Rates, 2nd Edition. *Trans. Institusion Chem. Eng.* **2003**, *81* (Part A), 285. https://doi.org/10.1002/ajmg.a.10488.

(8) Peters., F. Nucleation and Growth Rates from Shock Tube Experiments. *Atmos. Aerosols Nucleation* **1988**, *309*, 535–537.

(9) Schmitt, J. L.; Adams, G. W.; Zalabsky, R. A. Homogeneous Nucleation of Ethanol. *J. Chem. Phys.* **1982**, *77* (4), 2089–2097. https://doi.org/10.1063/1.444014.

(10) Wegener, P. P.; Mirabel, P. Homogeneous Nucleation in Supersaturated Vapors. *Naturwissenschaften* **1987**, *74* (3), 111–119. https://doi.org/10.1007/BF00366518.

(11) Davey, R. J.; Schroeder, S. L. M.; Ter Horst, J. H. Nucleation of Organic Crystals - A Molecular Perspective. *Angew. Chemie - Int. Ed.* **2013**, *52* (8), 2167–2179. https://doi.org/10.1002/anie.201204824.

(12) Xiao, Y.; Wang, J.; Huang, X.; Shi, H.; Zhou, Y.; Zong, S.; Hao, H.; Bao, Y.; Yin, Q. Determination Methods for Crystal

Nucleation Kinetics in Solutions. *Cryst. Growth Des.* **2018**, *18* (1), 540–551. https://doi.org/10.1021/acs.cgd.7b01223.

(13) Kobari, M.; Kubota, N.; Hirasawa, I. Deducing Primary Nucleation Parameters from Metastable Zone Width and Induction Time Data Determined with Simulation. *CrystEngComm* **2013**, *15* (6), 1199–1209. https://doi.org/10.1039/c2ce26679b.

(14) Kubota, N. Monte Carlo Simulation of Induction Time and Metastable Zone Width; Stochastic or Deterministic? *J. Cryst. Growth* **2018**, *485*, 1–7. https://doi.org/10.1016/j.jcrysgro.2017.12.031.

(15) Prado, S. C. C.; Rino, J. P.; Zanotto, E. D. Successful Test of the Classical Nucleation Theory by Molecular Dynamic Simulations of BaS. *Comput. Mater. Sci.* **2019**, *161* (February), 99–106. https://doi.org/10.1016/j.commatsci.2019.01.023.

(16) Nývlt, J. Kinetics of Nucleation in Solutions. *J. Cryst. Growth* **1968**, *3–4* (C), 377–383. https://doi.org/10.1016/0022-0248(68)90179-6.

(17) Kubota, N. The Concept of Metastable Zone; Is It Useful for the Design of a Batch Crystallizer ? **2004**, No. 690, 1–10.

(18) Kubota, N. A New Interpretation of Metastable Zone Widths Measured for Unseeded Solutions. *J. Cryst. Growth* **2008**, *310* (3), 629–634. https://doi.org/10.1016/j.jcrysgro.2007.11.123.

(19) Sangwal, K. A Novel Self-Consistent Nývlt-like Equation for Metastable Zone Width Determined by the Polythermal Method. *Cryst. Res. Technol.* **2009**, *44* (3), 231–247. https://doi.org/10.1002/crat.200800501.

(20) Sangwal, K. Novel Approach to Analyze Metastable Zone Width Determined by the Polythermal Method: Physical Interpretation of Various Parameters. *Cryst. Growth Des.* **2009**, *9* (2), 942–950. https://doi.org/10.1021/cg800704y.

(21) Camacho Corzo, D. M.; Borissova, A.; Hammond, R. B.; Kashchiev, D.; Roberts, K. J.; Lewtas, K.; More, I. Nucleation Mechanism and Kinetics from the Analysis of Polythermal Crystallisation Data: Methyl Stearate from Kerosene Solutions. *CrystEngComm* **2014**, *16* (6), 974–991. https://doi.org/10.1039/c3ce41098f.

(22) Kashchiev, D.; Borissova, A.; Hammond, R. B.; Roberts, K. J. Effect of Cooling Rate on the Critical Undercooling for Crystallization. *J. Cryst. Growth* **2010**, *312* (5), 698–704. https://doi.org/10.1016/j.jcrysgro.2009.12.031.

(23) Mullin, J. W. *Crystallization*; Butterworth Heinemann, 2001.

(24) Vekilov, P. G. Nucleation. *Cryst. Growth Des.* **2010**, *10*, 5007–5019. https://doi.org/10.1021/cg1011633.

(25) Mersmann, A. *Crystallization: A Technology Handbook*; Marcel Dekker AG, 2001. https://doi.org/10.1192/bjp.111.479.1009-a.

(26) Kashchiev, D. *Nucleation: Basic Theory With Applications*; Butterworth Heinemann, 2000.

(27) Kalikmanov, V. *Nucleation Theory*; Springer, 2012.

(28) Mokross, B. J. Nucleation Theory and Small System Thermodynamics. *Mater. Phys. Mech.* **2003**, *6* (1), 13–20.

(29) Bhamidi, V.; Kenis, P. J. A.; Zukoski, C. F. Probability of Nucleation in a Metastable Zone: Cooling Crystallization and Polythermal Method. *Cryst. Growth Des.* **2017**, *17* (11), 5823–5837. https://doi.org/10.1021/acs.cgd.7b00875.

(30) Anwar, J.; Zahn, D. Uncovering Molecular Processes in Crystal Nucleation and Growth by Using Molecular Simulation. *Angew. Chemie - Int. Ed.* **2011**, *50* (9), 1996–2013. https://doi.org/10.1002/anie.201000463.

(31) Julin, J.; Napari, I.; Merikanto, J.; Vehkamäki, H. A Thermodynamically Consistent Determination of Surface Tension of Small Lennard-Jones Clusters from Simulation and Theory. *J. Chem. Phys.* **2010**, *133* (4), 1–6. https://doi.org/10.1063/1.3456184.

(32) Benning, L. G. *New Perspectives on Mineral Nucleation and Growth*; 2017. https://doi.org/10.1007/978-3-319-45669-0.

(33) Vekilov, P. G. The Two-Step Mechanism of Nucleation of Crystals in Solution. *Nanoscale* **2010**, *2* (11), 2346–2357. https://doi.org/10.1039/c0nr00628a.

(34) Galkin, O.; Vekilov, P. G. Nucleation of Protein Crystals: Critical Nuclei, Phase Behavior, and Control Pathways. *J. Cryst. Growth* **2001**, *232* (1–4), 63–76. https://doi.org/10.1016/S0022-0248(01)01052-1.

(35) Karthika, S.; Radhakrishnan, T. K.; Kalaichelvi, P. A Review of Classical and Nonclassical Nucleation Theories. *Cryst. Growth Des.* **2016**, *16* (11), 6663–6681. https://doi.org/10.1021/acs.cgd.6b00794.

(36) Candoni, N.; Grossier, R.; Hammadi, Z.; Morin, R.; Veesler, S. Practical Physics Behind Growing Crystals of Biological Macromolecules. *Protein Pept. Lett.* **2012**, *19* (7), 714–724. https://doi.org/10.2174/092986612800793136.

(37) Kashchiev, D.; Verdoes, D.; van Rosmalen, G. M. Induction Time and Metastability Limit in New Phase Formation. *J. Cryst. Growth* **1991**, *110* (3), 373–380. https://doi.org/10.1016/0022-0248(91)90273-8.

(38) Ostwald, W. Studien Über Die Bildun Und Umwandlung Fester Körper. *Zeitschrift für Phys. Chemie* **1897**, *22*, 289–330.

(39) Myerson, A. S.; Anderson, S. R.; Bennett, R. C.; Green, D.; Karpinski, P. *Handbook of Industrial Crystallization*, 2nd Editio.; Elsevier Science & Technology Books, 2001. https://doi.org/10.1017/9781139026949.

(40) Mitchell, C. A.; Yu, L.; Ward, M. D. Selective Nucleation and Discovery of Organic Polymorphs through Epitaxy with Single Crystal Substrates. *J. Am. Chem. Soc.* **2001**, *123* (44), 10830–10839. https://doi.org/10.1021/ja004085f.

(41) Liu, J.; Nicholson, C. E.; Cooper, S. J. Direct Measurement of Critical Nucleus Size in Confined Volumes. *Langmuir* **2007**, *23* (13), 7286–7292. https://doi.org/10.1021/la063650a.

(42) Mitchell, N. A.; Frawley, P. J.; Ó'Ciardhá, C. T. Nucleation Kinetics of Paracetamolethanol Solutions from Induction Time Experiments Using Lasentec FBRM®. *J. Cryst. Growth* **2011**, *321* (1), 91–99. https://doi.org/10.1016/j.jcrysgro.2011.02.027.

(43) Barrett, P.; Glennon, B. Characterizing the Metastable Zone Width and Solubility Curve Using Lasentec FBRM and PVM. *Trans. Institusion Chem. Eng.* **2002**, *80* (October), 799–805. https://doi.org/10.1205/026387602320776876.

(44) Simon, L. L.; Nagy, Z. K.; Hungerbuhler, K. Endoscopy-Based in Situ Bulk Video Imaging of Batch Crystallization Processes. *Org. Process Res. Dev.* **2009**, *13* (6), 1254–1261. https://doi.org/10.1021/op900019b.

(45) Rossi, D.; Gavriilidis, A.; Kuhn, S.; Candel, M. A.; Jones, A. G.; Price, C.; Mazzei, L. Adipic Acid Primary Nucleation Kinetics from Probability Distributions in Droplet-Based Systems under Stagnant and Flow Conditions. *Cryst. Growth Des.* **2015**, *15* (4), 1784–1791. https://doi.org/10.1021/cg501836e.

(46) Chen, K.; Goh, L.; He, G.; Kenis, P. J. A.; Zukoski, C. F.; Braatz, R. D. Identification of Nucleation Rates in Droplet-Based Microfluidic Systems. *Chem. Eng. Sci.* **2012**, *77*, 235–241. https://doi.org/10.1016/j.ces.2012.03.026.

(47) Smith, K. W.; Cain, F. W.; Talbot, G. Crystallisation of 1,3-Dipalmitoyl-2-Oleoylglycerol and Tripalmitoylglycerol and Their Mixtures from Acetone. *Eur. J. Lipid Sci. Technol.* **2005**, *107* (9), 583–593. https://doi.org/10.1002/ejlt.200501169.

(48) He, G.; Tjahjono, M.; Chow, P. S.; Tan, R. B. H.; Garland, M. In Situ Determination of Metastable Zone Width Using Dielectric Constant Measurement. *Org. Process Res. Dev.* **2010**, *14* (6), 1469–1472. https://doi.org/10.1021/op100182s.

(49) Fujiwara, M.; Chow, P. S.; Ma, D. L.; Braatz, R. D. Paracetamol Crystallization Using Laser Backscattering and ATR-FTIR Spectroscopy: Metastability, Agglomeration, and Control. *Cryst. Growth Des.* **2002**, *2* (5), 363–370. https://doi.org/10.1021/cg0200098.

(50) Kim, J. W.; Kim, J.; Lee, K. D.; Koo, K. K. Evaluation of Nucleation Rate by In-Situ Focused Beam Reflectance Measurement in an Unseeded Batch Cooling Crystallization. *Cryst. Res. Technol.* **2013**, *48* (12), 1097–1105. https://doi.org/10.1002/crat.201300288.

(51) Liu, J.; Rasmuson, Å. C. Influence of Agitation and Fluid Shear on Primary Nucleation in Solution. *Cryst. Growth Des.* **2013**, *13* (10), 4385–4394. https://doi.org/10.1021/cg4007636.

(52) Yang, H.; Rasmuson, Å. C. Nucleation of Butyl Paraben in Different Solvents. *Cryst. Growth Des.* **2013**, *13* (10), 4226–4238. https://doi.org/10.1021/cg400177u.

(53) Cedeno, R.; Maosoongnern, S.; Flood, A. Direct Measurements of Primary Nucleation Rates of P-Aminobenzoic Acid and Glutamic Acid and Comparison with Predictions from Induction Time Distributions. *Ind. Eng. Chem. Res.* **2018**, *57* (51), 17504–17515. https://doi.org/10.1021/acs.iecr.8b03625.

(54) Liang, K.; White, G.; Wilkinson, D.; Ford, L. J.; Roberts, K. J.; Wood, W. M. L. An Examination into the Effect of Stirrer Material and Agitation Rate on the Nucleation of L-Glutamic Acid Batch Crystallized from Supersaturated Aqueous Solutions. *Cryst. Growth Des.* **2004**, *4* (5), 1039–1044. https://doi.org/10.1021/cg034096v.

(55) Titiz-Sargut, S.; Ulrich, J. Application of a Protected Ultrasound Sensor for the Determination of the Width of the Metastable Zone. *Chem. Eng. Process. Process Intensif.* **2003**, *42* (11), 841–846. https://doi.org/10.1016/S0255-2701(02)00215-5.

(56) Prasad, R.; Dalvi, S. V. Sonocrystallization: Monitoring and Controlling Crystallization Using Ultrasound. *Chem. Eng. Sci.* **2020**, *226*, 115911. https://doi.org/10.1016/j.ces.2020.115911.

(57) Helmdach, L.; Feth, M. P.; Ulrich, J. Application of Ultrasound Measurements as Pat Tools for Industrial Crystallization Process Development of Pharmaceutical Compounds. *Org. Process Res. Dev.* **2015**, *19* (1), 110–121. https://doi.org/10.1021/op4001803.

(58) Genceli, F. E.; Himawan, C.; Witkamp, G. J. Inline Determination of Supersaturation and Metastable Zone Width of MgSO4.12H2O with Conductivity and Refractive Index Measurement Techniques. *J. Cryst. Growth* **2005**, *275* (1–2). https://doi.org/10.1016/j.jcrysgro.2004.11.162.

(59) Mullin, J. W.; Jancic, S. J. Interpretation of the Metastable Zone Width. *Trans. Institusion Chem. Eng.* **1979**, *57*, 188–193.

(60) Marciniak, B. Density and Ultrasonic Velocity of Undersaturated and Supersaturated Solutions of Fluoranthene in Trichloroethylene, and Study of Their Metastable Zone Width. *J. Cryst. Growth* **2002**, *236* (1–3), 347–356. https://doi.org/10.1016/S0022-0248(01)02088-7.

(61) Darcy, P. A.; Wiencek, J. M. Estimating Lysozyme Crystallization Growth Rates and Solubility from Isothermal Microcalorimetry. *Acta Crystallogr. Sect. D Biol. Crystallogr.* **1998**, *54* (6 PART II), 1387–1394. https://doi.org/10.1107/s0907444998006052.

(62) Maggioni, G. M.; Mazzotti, M. Modelling the Stochastic Behaviour of Primary Nucleation. *Faraday Discuss.* **2015**, *179*, 359–382. https://doi.org/10.1039/c4fd00255e.

(63) Toschev, S.; Milchev, A.; Stoyanov, S. On Some Probabilistic Aspects of the Nucleation Process. *J. Cryst. Growth* **1972**, *13–14* (C), 123–127. https://doi.org/10.1016/0022-0248(72)90073-5.

(64) Bhamidi, V.; Kenis, P. J. A.; Zukoski F, C. F. Probability of Nucleation in a Metastable Zone: Induction Supersaturation and Implications. *Cryst. Growth Des.* **2017**, *17*, 1132–1145. https://doi.org/10.1021/acs.cgd.6b01529.

(65) Maggioni, G. M.; Bosetti, L.; Dos Santos, E.; Mazzotti, M. Statistical Analysis of Series of Detection Time Measurements for the Estimation of Nucleation Rates. *Cryst. Growth Des.* **2017**, *17* (10), 5488–5498. https://doi.org/10.1021/acs.cgd.7b01014.

(66) Goh, L.; Chen, K.; Bhamidi, V.; He, G.; Kee, N. C. S.; Kenis, P. J. A.; Zukoski, C. F.; Braatz, R. D. A Stochastic Model for Nucleation Kinetics Determination in Droplet-Based Microfluidic Systems. *Cryst. Growth Des.* **2010**, *10* (6), 2515–2521. https://doi.org/10.1021/cg900830y.

(67) Tamura, R.; Miyata, M. *Advances in Organic Crystal Chemistry: Comprehensive Reviews 2015*; 2015. https://doi.org/10.1007/978-4-431-55555-1.

(68) Steendam, R. R. E.; Keshavarz, L.; Blijlevens, M. A. R.; De Souza, B.; Croker, D. M.; Frawley, P. J. Effects of Scale-Up on the Mechanism and Kinetics of Crystal Nucleation. *Cryst. Growth Des.* **2018**, *18* (9), 5547–5555. https://doi.org/10.1021/acs.cgd.8b00857.

(69) Xiao, Y.; Tang, S. K.; Hao, H.; Davey, R. J.; Vetter, T. Quantifying the Inherent Uncertainty Associated with Nucleation Rates Estimated from Induction Time Data Measured in Small Volumes. *Cryst. Growth Des.* **2017**, *17* (5), 2852–2863. https://doi.org/10.1021/acs.cgd.7b00372.

(70) Kadam, S. S.; Kramer, H. J. M.; Ter Horst, J. H. Combination of a Single Primary Nucleation Event and Secondary Nucleation in Crystallization Processes. *Cryst. Growth Des.* **2011**, *11* (4), 1271–1277. https://doi.org/10.1021/cg101504c.

(71) Kadam, S. S.; Kulkarni, S. A.; Coloma Ribera, R.; Stankiewicz, A. I.; ter Horst, J. H.; Kramer, H. J. M. A New View on the Metastable Zone Width during Cooling Crystallization. *Chem. Eng. Sci.* **2012**, *72*, 10–19.

https://doi.org/10.1016/j.ces.2012.01.002.

(72) Ildefonso, M.; Revalor, E.; Punniam, P.; Salmon, J. B.; Candoni, N.; Veesler, S. Nucleation and Polymorphism Explored via an Easy-to-Use Microfluidic Tool. *J. Cryst. Growth* **2012**, *342* (1), 9–12. https://doi.org/10.1016/j.jcrysgro.2010.11.098.

(73) Wang, T.; Lu, H.; Wang, J.; Xiao, Y.; Zhou, Y.; Bao, Y.; Hao, H. Recent Progress of Continuous Crystallization. *J. Ind. Eng. Chem.* **2017**, *54*, 14–29. https://doi.org/10.1016/j.jiec.2017.06.009.

(74) Gherras, N.; Fevotte, G. *On the Use of Process Analytical Technologies and Population Balance Equations for the Estimation of Crystallization Kinetics. A Case Study.*; 2012; Vol. 58. https://doi.org/10.1002/aic.12776.

(75) Preckshot, G. W.; Brown, G. G. Unknown. *Ind. Eng. Chem.* **1952**, *44*, 1314–1321.

(76) Söhnel, O. .; Nývlt, J. Evaluation of Experimental Data on Width of Metastable Region in Aqueous Solutions. *Collect. Czechoslov. Chem. Commun.* **1975**, *40* (1), 511–518.

(77) Harano, Y.; Nakano, K.; Saito, M.; Imoto, T. Nucleation Rate of Potassium Chlorate from Quiescent Supersaturated Aqueous Solution. *J. Chem. Eng. Japan* **1976**, *9* (5), 373–377. https://doi.org/10.1252/jcej.9.373.

(78) Harano, Y.; Oota, K. Measurement of Crystallization of Potassium Bromate from Its Quiescent Aqueous Solution by Differential Scanning Calorimeter. *J. Chem. Eng. Japan* **1978**, *11* (2), 119–124. https://doi.org/https://doi.org/10.1252/jcej.11.119.

(79) Harano, Y.; Yamamoto, H.; Miura, T.; Yamamoto, H. Non-Isothermal Analysis of Nucleation of KBrO3 by Differential Scanning Calorimetry. *J. Chem. Eng. Japan* **1981**, *14* (6), 439–444. https://doi.org/10.1252/jcej.14.439.

(80) Mersmann, A.; Bartosch, K. How to Predict the Metastable Zone Width. *J. Cryst. Growth* **1998**, *183* (1–2), 240–250. https://doi.org/10.1016/S0022-0248(97)00417-X.

(81) Kim, K. J.; Mersmann, A. Estimation of Metastable Zone Width in Different Nucleation Processes. *Chem. Eng. Sci.* **2001**, *56* (7), 2315–2324. https://doi.org/10.1016/S0009-2509(00)00450-4.

(82) Nagy, Z. K.; Fujiwara, M.; Woo, X. Y.; Braatz, R. D. Determination of the Kinetic Parameters for the Crystallization of Paracetamol from Water Using Metastable Zone Width Experiments. *Ind. Eng. Chem. Res.* **2008**, *47* (4), 1245–1252. https://doi.org/10.1021/ie060637c.

(83) Shiau, L. D.; Lu, T. S. A Model for Determination of the Interfacial Energy from the Induction Time or Metastable Zone Width Data Based on Turbidity Measurements. *CrystEngComm* **2014**, *16* (41), 9743–9752. https://doi.org/10.1039/c4ce01245c.

(84) Shiau, L. D. Determination of the Nucleation and Growth Kinetics for Aqueous L-Glycine Solutions from the Turbidity Induction Time Data. *Crystals* **2018**, *8* (11). https://doi.org/10.3390/cryst8110403.

(85) Nývlt, J.; Rychlý, R.; Gottfried, J.; Wurzelová, J. Metastable Zone-Width of Some Aqueous Solutions. *J. Cryst. Growth* **1970**, *6* (2), 151–162. https://doi.org/10.1016/0022-0248(70)90034-5.

(86) Janse, A. H.; de Jong, E. J. On the Metastable Zone,. *Trans. Institusion Chem. Eng.* **1978**, *56*, 87–163.

(87) Hulburt, H. M. Die Induktionsperiode Bei Der Chargen-Kristallisation Und Beim Ausfällen. *Chemie Ing. Tech.* **1975**, *47* (9), 373–375.

(88) Jiang, S. An Examination of Sonocrystallization Kinetics of L-Glutamic Acid, University of Leeds, 2012.

(89) Mitchell, N. A.; Frawley, P. J. Nucleation Kinetics of Paracetamol Ethanol Solutions from Metastable Zone Widths. *J. Cryst. Growth* **2010**, *312* (19), 2740–2746. https://doi.org/10.1016/j.jcrysgro.2010.05.043.

(90) Mersmann, A. Supersaturation and Nucleation. *Chem. Eng. Res. Des.* **1996**, *74* (7), 812–820.

(91) Nielsen, A. E. *Kinetics of Precipitation*, 1st ed.; Pergamon Press: Oxford, New York, 1964.

(92) Kashchiev, D.; Borissova, A.; Hammond, R. B.; Roberts, K. J. Dependence of the Critical Undercooling for Crystallization on the Cooling Rate. *J. Phys. Chem. B* **2010**, *114* (16), 5441–5446. https://doi.org/10.1021/jp100202m.

(93) Wohlgemuth, K.; Schembecker, G. Modeling Induced Nucleation Processes during Batch Cooling Crystallization: A Sequential Parameter Determination Procedure. *Comput. Chem. Eng.* **2013**, *52*, 216–229. https://doi.org/10.1016/j.compchemeng.2012.12.001.

(94) Shiau, L. D. Investigations into the Influence of Solvents on the Nucleation Kinetics for Isonicotinamide, Lovastatin, and Phenacetin. *ACS Omega* **2019**, *4* (17), 17352–17358. https://doi.org/10.1021/acsomega.9b02102.

(95) Dugua, J.; Simon, B. Crystallization of Sodium Perborate from Aqueous Solutions. *J. Cryst* **1978**, *44*, 265–279.

(96) Boistelle, R.; Astier, J. P. Crystallization Mechanisms in Solution. *J. Cryst. Growth* **1988**, *90* (1–3), 14–30. https://doi.org/10.1016/0022-0248(88)90294-1.

(97) Shi, H. H.; Xiao, Y.; Ferguson, S.; Huang, X.; Wang, N.; Hao, H. X. Progress of Crystallization in Microfluidic Devices. *Lab Chip* **2017**, *17* (13), 2167–2185. https://doi.org/10.1039/c6lc01225f.

(98) Whitesides, G. M. The Origins and the Future of Microfluidics. *Nature* **2006**, *442* (7101), 368–373. https://doi.org/10.1038/nature05058.

(99) Leng, J.; Salmon, J. B. Microfluidic Crystallization. *Lab Chip* **2009**, *9* (1), 24–34. https://doi.org/10.1039/b807653g.

(100) Chen, J.; Sarma, B.; Evans, J. M. B.; Myerson, A. S. Pharmaceutical Crystallization. *Cryst. Growth Des.* **2011**, *11* (4), 887–895. https://doi.org/10.1021/cg101556s.

(101) Laval, P.; Salmon, J. B.; Joanicot, M. A Microfluidic Device for Investigating Crystal Nucleation Kinetics. *J. Cryst. Growth* **2007**, *303* (2), 622–628. https://doi.org/10.1016/j.jcrysgro.2006.12.044.

(102) Brandel, C.; ter Horst, H. J. Measuring Induction Times and Crystal Nucleation Rates. *R. Soc. Chem.* **2013**, No. 207890, 1–15. https://doi.org/10.1039/b000000x.

(103) Nappo, V. Experimental Study on the Influence of Fluid Dynamics and Mixing on Crystallisation of PABA in Multiphase Flow Systems, University College London.

(104) Tsekova, D.; Dimitrova, S.; Nanev, C. N. Heterogeneous Nucleation (and Adhesion) of Lysozyme Crystals. *J. Cryst. Growth* **1999**, *196* (2–4), 226–233. https://doi.org/10.1016/S0022-0248(98)00827-6.

(105) Galkin, O.; Vekilov, P. G. Direct Determination of the Nucleation Rates of Protein Crystals. *J. Phys. Chem. B* **1999**, *103* (49), 10965–10971. https://doi.org/10.1021/jp992786x.

(106) Nanev, C. N.; Hodzhaoglu, F. V.; Dimitrov, I. L. Kinetics of Insulin Crystal Nucleation, Energy Barrier, and Nucleus Size. *Cryst. Growth Des.* **2011**, *11* (1), 196–202. https://doi.org/10.1021/cg1011499.

(107) Ildefonso, M.; Candoni, N.; Veesler, S. Using Microfluidics for Fast, Accurate Measurement of Lysozyme Nucleation Kinetics. *Cryst. Growth Des.* **2011**, *11* (5), 1527–1530. https://doi.org/10.1021/cg101431g.

(108) Dixit, N. M.; Kulkarni, A. M.; Zukoski, C. F. Comparison of Experimental Estimates and Model Predictions of Protein Crystal Nucleation Rates. *Colloids Surfaces A Physicochem. Eng. Asp.* **2001**, *190* (1–2), 47–60. https://doi.org/10.1016/S0927-7757(01)00664-1.

(109) Lounaci, M.; Chen, Y.; Rigolet, P. Channel Height Dependent Protein Nucleation and Crystal Growth in Microfluidic Devices. *Microelectron. Eng.* **2010**, *87* (5–8), 750–752. https://doi.org/10.1016/j.mee.2009.11.154.

(110) Turnbull, D.; Vonnegut, B. Nucleation Catalysis. *Ind. Eng. Chem.* **1952**, *44* (6), 1292–1298. https://doi.org/10.1021/ie50510a031.

(111) Vonnegut, B. Variation with Temperature of the Nucleation Rate of Supercooled Liquid Tin and Water Drops. *J. Colloid Sci.* **1948**, *3* (6), 563–569.

(112) Liu, K.; Chen, Y. C.; Tseng, H. R.; Shen, C. K. F.; Van Dam, R. M. Microfluidic Device for Robust Generation of Two-Component Liquid-in-Air Slugs with Individually Controlled Composition. *Microfluid. Nanofluidics* **2010**, *9* (4–5), 933–943. https://doi.org/10.1007/s10404-010-0617-0.

(113) Suea-Ngam, A.; Howes, P. D.; Srisa-Art, M.; Demello, A. J. Droplet Microfluidics: From Proof-of-Concept to Real-World Utility? *Chem. Commun.* **2019**, *55* (67), 9895–9903. https://doi.org/10.1039/c9cc04750f.

(114) Zhu, P.; Wang, L. Passive and Active Droplet Generation with Microfluidics: A Review. *Lab Chip* **2017**, *17* (1), 34–75. https://doi.org/10.1039/C6LC01018K.

(115) Grossier, R.; Hammadi, Z.; Morin, R.; Magnaldo, A.; Veesler, S. Generating Nanoliter to Femtoliter Microdroplets with Ease. *Appl. Phys. Lett.* **2011**, *98* (9), 4–7. https://doi.org/10.1063/1.3560453.

(116) Teychené, S.; Biscans, B. Crystal Nucleation in a Droplet Based Microfluidic Crystallizer. *Chem. Eng. Sci.* **2012**, *77*, 242–248. https://doi.org/10.1016/j.ces.2012.01.036.

(117) Anna, S. L. Droplets and Bubbles in Microfluidic Devices. *Annu. Rev. Fluid Mech.* **2016**, *48* (1), 285–309. https://doi.org/10.1146/annurev-fluid-122414-034425.

(118) Laval, P.; Crombez, A.; Salmon, J. B. Microfluidic Droplet Method for Nucleation Kinetics Measurements. *Langmuir* **2009**, *25* (3), 1836–1841. https://doi.org/10.1021/la802695r.

(119) Fatemi, N.; Devos, C.; De Cordt, G.; Van Gerven, T.; Kuhn, S. Effect of Sodium Dodecyl Sulfate on the Continuous Crystallization in Microfluidic Devices Using Microbubbles. *Chem. Eng. Technol.* **2019**, *42* (10), 1–9. https://doi.org/10.1002/ceat.201900172.

(120) Han, D.; Wang, Y.; Yang, Y.; Gong, T.; Chen, Y.; Gong, J. Revealing the Role of a Surfactant in the Nucleation and Crystal Growth of Thiamine Nitrate: Experiments and Simulation Studies. *CrystEngComm* **2019**, *21* (23), 3576–3585. https://doi.org/10.1039/c9ce00325h.

(121) Fatemi, N.; Dong, Z.; Van Gerven, T.; Kuhn, S. Microbubbles as Heterogeneous Nucleation Sites for Crystallization in Continuous Microfluidic Devices. *Langmuir* **2019**, *35* (1), 60–69. https://doi.org/10.1021/acs.langmuir.8b03183.

(122) Dos Santos, E. C.; Maggioni, G. M.; Mazzotti, M. Statistical Analysis and Nucleation Parameter Estimation from Nucleation Experiments in Flowing Microdroplets. *Cryst. Growth Des.* **2019**, *19* (11), 6159–6174. https://doi.org/10.1021/acs.cgd.9b00562.

(123) Teychené, S.; Biscans, B. Microfluidic Device for the Crystallization of Organic Molecules in Organic Solvents. *Cryst. Growth Des.* **2011**, *11* (11), 4810–4818. https://doi.org/10.1021/cg2004535.

(124) Pound, G. M.; Mer, V. K. L. Kinetics of Crystalline Nucleus Formation in Supercooled Liquid Tin. *J. Am. Chem. Soc.* **1952**, *74* (9), 2323–2332. https://doi.org/10.1021/ja01129a044.

(125) Akella, S. V.; Mowitz, A.; Heymann, M.; Fraden, S. Emulsion-Based Technique to Measure Protein Crystal Nucleation Rates of Lysozyme. *Cryst. Growth Des.* **2014**, *14* (9), 4487–4509. https://doi.org/10.1021/cg500562r.

(126) The Pound and La Mer Model Does Not Predict That the "Slow" Nucleation Rate Is Only Due to Homogeneous Nucleation.

(127) Nappo, V.; Sullivan, R.; Davey, R.; Kuhn, S.; Gavriilidis, A.; Mazzei, L. Effect of Shear Rate on Primary Nucleation of Para-Amino Benzoic Acid in Solution under Different Fluid Dynamic Conditions. *Chem. Eng. Res. Des.* **2018**, *136*, 48–56. https://doi.org/10.1016/j.cherd.2018.04.039.

(128) Chen, D. L.; Gerdts, G. J.; Ismagilov, R. F. Using Microfluidics to Observe the Effect of Mixing on Nucleation of Protein Crystals. *J. Am. Chem. Soc.* **2005**, *127* (27), 9672–9673. https://doi.org/10.1021/ja052279v.

(129) Galkin, O.; Vekilov, P. G. Are Nucleation Kinetics of Protein Crystals Similar to Those of Liquid Droplets? *J. Am. Chem. Soc.* **2000**, *122* (1), 156–163. https://doi.org/10.1021/ja9930869.

(130) Knezic, D.; Zaccaro, J.; Myerson, A. S. Nucleation Induction Time in Levitated Droplets. *J. Phys. Chem. B* **2004**, *108* (30), 10672–10677. https://doi.org/10.1021/jp049586s.

(131) Shim, J.; Cristobal, G.; Link, D. R.; Thorsen, T.; Fraden, S. Using Microfluidics to Decouple Nucleation and Growth of Protein Crystals. *Cryst. Growth Des.* **2007**, *23* (1), 1–7. https://doi.org/10.1021/cg700688f.

(132) Dombrowski, R. D.; Litster, J. D.; Wagner, N. J.; He, Y. Crystallization of Alpha-Lactose Monohydrate in a Drop-Based Microfluidic Crystallizer. *Chem. Eng. Sci.* **2007**, *62* (17), 4802–4810. https://doi.org/10.1016/j.ces.2007.05.033.

(133) Selimović, Š.; Jia, Y.; Fraden, S. Measuring the Nucleation Rate of Lysozyme Using Microfluidics. *Cryst. Growth Des.* **2009**, *9* (4), 1806–1810. https://doi.org/10.1021/cg800990k.

(134) Talreja, S.; Kim, D. Y.; Mirarefi, A. Y.; Zukoski, C. F.; Kenis, P. J. A. Screening and Optimization of Protein Crystallization Conditions through Gradual Evaporation Using a Novel Crystallization Platform. *J. Appl. Crystallogr.* **2005**, *38* (6), 988–995.

https://doi.org/10.1107/S0021889805031572.

(135) Ildefonso, M.; Candoni, N.; Veesler, S. Heterogeneous Nucleation in Droplet-Based Nucleation Measurements. *Cryst. Growth Des.* **2013**, *13* (5), 2107–2110. https://doi.org/10.1021/cg4001686.

(136) Wantha, L.; Flood, A. E. Nucleation Kinetics of the γ-Polymorph of DL-Methionine. *Chem. Eng. Technol.* **2012**, *35* (6), 1024–1030. https://doi.org/10.1002/ceat.201100682.

(137) Lu, J.; Litster, J. D.; Nagy, Z. K. Nucleation Studies of Active Pharmaceutical Ingredients in an Air-Segmented Microfluidic Drop-Based Crystallizer. *Cryst. Growth Des.* **2015**, *15* (8), 3645–3651. https://doi.org/10.1021/acs.cgd.5b00150.

(138) Zhang, S.; Ferté, N.; Candoni, N.; Veesler, S. Versatile Microfluidic Approach to Crystallization. *Org. Process Res. Dev.* **2015**, *19* (12), 1837–1841. https://doi.org/10.1021/acs.oprd.5b00122.

(139) Selzer, D.; Spiegel, B.; Kind, M. A Generic Polycarbonate Based Microfluidic Tool to Study Crystal Nucleation in Microdroplets. *J. Cryst. Process Technol.* **2018**, *08* (01), 1–17. https://doi.org/10.4236/jcpt.2018.81001.

(140) Ferreira, J.; Castro, F.; Rocha, F.; Kuhn, S. Protein Crystallization in a Droplet-Based Microfluidic Device: Hydrodynamic Analysis and Study of the Phase Behaviour. *Chem. Eng. Sci.* **2018**, *191*, 232–244. https://doi.org/10.1016/j.ces.2018.06.066.

(141) Cruz-Cabeza, A. J.; Davey, R. J.; Sachithananthan, S. S.; Smith, R.; Tang, S. K.; Vetter, T.; Xiao, Y. Aromatic Stacking-a Key Step in Nucleation. *Chem. Commun.* **2017**, *53* (56), 7905–7908. https://doi.org/10.1039/c7cc02423a.

(142) Pino-García, O.; Rasmuson, Å. C. Primary Nucleation of Vanillin Explored by a Novel Multicell Device. *Ind. Eng. Chem. Res.* **2003**, *42* (20), 4899–4909. https://doi.org/10.1021/ie0210412.

(143) Ramakers, L. A. I.; McGinty, J.; Beckmann, W.; Levilain, G.; Lee, M.; Wheatcroft, H.; Houson, I.; Sefcik, J. Investigation of Metastable Zones and Induction Times in Glycine Crystallization across Three Different Antisolvents. *Cryst. Growth Des.* **2020**, *20* (8), 4935–4944. https://doi.org/10.1021/acs.cgd.9b01493.

(144) Juárez-Martínez, G.; Steinmann, P.; Roszak, A. W.; Isaacs, N. W.; Cooper, J. M. High-Throughput Screens for Postgenomics: Studies of Protein Crystallization Using Microsystems Technology. *Anal. Chem.* **2002**, *74* (14), 3505–3510. https://doi.org/10.1021/ac0112519.

(145) Sullivan, R. A.; Davey, R. J.; Sadiq, G.; Dent, G.; Back, K. R.; Ter Horst, J. H.; Toroz, D.; Hammond, R. B. Revealing the Roles of Desolvation and Molecular Self-Assembly in Crystal Nucleation from Solution: Benzoic and p -Aminobenzoic Acids. *Cryst. Growth Des.* **2014**, *14* (5), 2689–2696. https://doi.org/10.1021/cg500441g.

(146) Sun, W.; Booth, S.; Myerson, A.; Hughes, C.; Pan, H.; Coquerel, G.; Brandel, C.; Meekes, H.; Mazzotti, M.; Fabian, L.; et al. Time and Space Resolved Methods: General Discussion. *Faraday Discuss.* **2015**, *179*, 247–267. https://doi.org/10.1039/c5fd90037a.

(147) Kulkarni, S. A.; Kadam, S. S.; Meekes, H.; Stankiewicz, A. I.; Ter Horst, J. H. Crystal Nucleation Kinetics from Induction Times and Metastable Zone Widths. *Cryst. Growth Des.* **2013**, *13* (6), 2435–2440. https://doi.org/10.1021/cg400139t.

(148) Lindenberg, C.; Mazzotti, M. Effect of Temperature on the Nucleation Kinetics of α L-Glutamic Acid. *J. Cryst. Growth* **2009**, *311* (4), 1178–1184. https://doi.org/10.1016/j.jcrysgro.2008.12.010.

(149) Schöll, J.; Vicum, L.; Müller, M.; Mazzotti, M. Precipitation of L-Glutamic Acid: Determination of Nucleation Kinetics. *Chem. Eng. Technol.* **2006**, *29* (2), 257–264. https://doi.org/10.1002/ceat.200500369.

(150) Nordström, F. L.; Svärd, M.; Rasmuson, Å. C. Primary Nucleation of Salicylamide: The Influence of Process Conditions and Solvent on the Metastable Zone Width. *CrystEngComm* **2013**, *15* (36), 7285–7297. https://doi.org/10.1039/c3ce40619a.

(151) Grossier, R.; Hammadi, Z.; Morin, R.; Veesler, S. Predictive Nucleation of Crystals in Small Volumes and Its Consequences. *Phys. Rev. Lett.* **2011**, *107* (2). https://doi.org/10.1103/PhysRevLett.107.025504.

(152) Veintemillas-Verdaguer, S.; Esteban, S. O.; Herrero, M. A. The Effect of Stirring on Sodium Chlorate Crystallization under Symmetry Breaking Conditions. *J. Cryst. Growth* **2007**, *303* (2), 562–567. https://doi.org/10.1016/j.jcrysgro.2007.01.014.

(153) Forsyth, C.; Mulheran, P. A.; Forsyth, C.; Haw, M. D.; Burns, I. S.; Sefcik, J. Influence of Controlled Fluid Shear on Nucleation Rates in Glycine Aqueous Solutions. *Cryst. Growth Des.* **2015**, *15* (1), 94–102. https://doi.org/10.1021/cg5008878.

(154) Forsyth, C.; Burns, I. S.; Mulheran, P. A.; Sefcik, J. Scaling of Glycine Nucleation Kinetics with Shear Rate and Glass-Liquid Interfacial Area. *Cryst. Growth Des.* **2016**, *16* (1), 136–144. https://doi.org/10.1021/acs.cgd.5b01042.

(155) Mullin, J. W.; Raven, K. . Influence of Mechanical Agitation on the Nucleation Of Some Aqueous Salt Solutions. *Nat. Int. J. Sci.* **1962**, *196*, 1048–1050. https://doi.org/https://doi.org/10.1038/1961048b0.

(156) Anwar, J.; Khan, S.; Lindfors, L. Secondary Crystal Nucleation: Nuclei Breeding Factory Uncovered. *Angew. Chemie - Int. Ed.* **2015**, *54* (49), 14681–14684. https://doi.org/10.1002/anie.201501216.

(157) Cui, Y.; Myerson, A. S. Experimental Evaluation of Contact Secondary Nucleation Mechanisms. *Cryst. Growth Des.* **2014**, *14* (10), 5152–5157. https://doi.org/10.1021/cg500861f.

(158) Qian, R. Y.; Botsaris, G. D. Nuclei Breeding from a Chiral Crystal Seed of NaClO3. *Chem. Eng. Sci.* **1998**, *53* (9), 1745–1756. https://doi.org/10.1016/S0009-2509(98)00040-2.

(159) Agrawal, S. G.; Paterson, A. H. J. Secondary Nucleation: Mechanisms and Models. *Chem. Eng. Commun.* **2015**, *202* (5), 698–706. https://doi.org/10.1080/00986445.2014.969369.

(160) Erdemir, D.; Lee, A. Y.; Myerson, A. S. *Handbook of Industrial Crystallization: Chapter 3 Crystal Nucleation*; Cambridge University Press, 2019. https://doi.org/10.1017/9781139026949.003.

(161) Myerson, A. S.; Erdemir, D.; Lee, A. Y. *Handbook of Industrial Crystallization*, Third Edit.; Cambridge University Press, 2019.

(162) Bosetti, L.; Mazzotti, M. Study of Secondary Nucleation by Attrition of Potassium Alum Crystals Suspended in Different Solvents. *Cryst. Growth Des.* **2020**, *20* (4), 2570–2577. https://doi.org/10.1021/acs.cgd.9b01700.

(163) Briuglia, M. L.; Sefcik, J.; Horst, J. H. T. Measuring Secondary Nucleation through Single Crystal Seeding. *Cryst. Growth Des.* **2019**, *19* (1), 421–429. https://doi.org/10.1021/acs.cgd.8b01515.

(164) Tyrrell, R.; De Souza, B.; Frawley, P. J. Particle Breakage: Limiting Conditions for Crystal-Crystallizer Collisions. *Cryst. Growth Des.* **2018**, *18* (2), 617–622. https://doi.org/10.1021/acs.cgd.7b00125.

(165) Buhse, T.; Durand, D.; Kondepudi, D.; Laudadio, J.; Spilker, S. Chiral Symmetry Breaking in Crystallization: The Role of Convection. *Phys. Rev. Lett.* **2000**, *84* (19), 4405–4408. https://doi.org/10.1103/PhysRevLett.84.4405.

(166) Agrawal, S. G.; Paterson, A. H. J. Secondary Nucleation: Mechanisms and Models. *Chem. Eng. Commun.* **2015**, *202* (5), 698–706. https://doi.org/10.1080/00986445.2014.969369.

(167) Mullin, J. W.; Leci, C. L. Evidence of Molecular Cluster Formation in Supersaturated Solutions of Citric Acid. *Philos. Mag.* **1969**, *19* (161), 1075–1077. https://doi.org/10.1080/14786436908225872.

(168) Gebauer, D.; Völkel, A.; Cölfen, H. Stable Prenucleation Calcium Carbonate Clusters. *Science (80-.).* **2008**, *322* (5909), 1819–1822. https://doi.org/10.1126/science.1164271.

(169) Chattopadhyay, S.; Erdemir, D.; Evans, J. M. B.; Ilavsky, J.; Amenitsch, H.; Segre, C. U.; Myerson, A. S. SAXS Study of the Nucleation of Glycine Crystals from a Supersaturated Solution. *Cryst. Growth Des.* **2005**, *5* (2), 523–527. https://doi.org/10.1021/cg0497344.

(170) Pan, W.; Vekilov, P. G.; Lubchenko, V. Origin of Anomalous Mesoscopic Phases in Protein Solutions. *J. Phys. Chem. B* **2010**, *114* (22), 7620–7630. https://doi.org/10.1021/jp100617w.

(171) Jawor-Baczynska, A.; Moore, B. D.; Sefcik, J. Effect of Mixing, Concentration and Temperature on the Formation of Mesostructured Solutions and Their Role in the Nucleation of DL-Valine Crystals. *Faraday Discuss.* **2015**, *179* (0), 141–154. https://doi.org/10.1039/c4fd00262h.

(172) Zimbitas, G.; Jawor-Baczynska, A.; Vesga, M. J.; Javid, N.; Moore, B. D.; Parkinson, J.; Sefcik, J. Investigation of Molecular and Mesoscale Clusters in Undersaturated Glycine Aqueous Solutions. *Colloids Surfaces A Physicochem. Eng. Asp.* **2019**, *579* (June), 123633. https://doi.org/10.1016/j.colsurfa.2019.123633.